Improving Brush Polymer Infrared 1-D Photonic Crystals via Linear Polymer Additives
Supporting Information

Robert J. Macfarlane, Bongkeun Kim, Byeongdu Lee, Raymond A. Weitekamp, Christopher M. Bates, Siu Fung Lee, Alice B. Chang, Kris T. Delaney, Glenn Frederickson, Harry A. Atwater, Robert H. Grubbs

Materials:

Unless otherwise noted, all solvents and reagents were purchased from VWR or Sigma-Aldrich. The ruthenium-based metathesis catalyst was obtained from Materia Inc. and stored in a drybox prior to use, and the RuO_4 SEM staining agent was obtained from Polysciences, Inc and stored at 4 °C. The ruthenium metathesis catalyst ($(H_2IMes)(pyr)_2(Cl)_2RuCHPh$) and PLA macromonomer initiator (N-(hydroxyethanyl)-cis-5-norbornene-exo-2,3-dicarboximide) were prepared as described previously (1). Dry solvents were purified by passing them through solvent purification columns, and 3,6-dimethyl-1,4-dioxane-2,5-dione was purified by sublimation under vacuum. All other solvents and chemicals were used without further purification unless otherwise noted.

General Information:

NMR spectra were recorded at room temperature on a Varian Inova 500 (at 500 MHz), and analyzed on MestReNova software. Gel permeation chromatography (GPC) was carried out in THF on two Plgel 10 μm mixed-B LS columns (Polymer Laboratories) connected in series with a miniDAWN TREOS multiangle laser light scattering (MALLS) detector, a ViscoStar viscometer and Optilab rex differential refractometer (all from Wyatt Technology). The dn/dc values used for the polylactide and polystyrene macromonomers were 0.050 and 0.180 respectively, and dn/dc values for the brush polymers and random copolymers were obtained for each injection by assuming 100% mass elution from the columns. SEM images were taken on a ZEISS 1550 VP

Field Emission SEM, and reflection measurements were performed on a Cary 5000 UV/Vis/NIR spectrophotometer, equipped with an 'integrating sphere' diffuse reflectance accessory (Internal DRA 1800); all reflection measurements were referenced to a LabSphere Spectralon 99% certified reflectance standard. The samples were illuminated through a Spectralon-coated aperature with a diameter of 1 cm, with a beam area of approximately 0.5 cm^2. The samples were scanned at a rate of 600 nm/min with a 1 nm data interval, with detector crossover (InGaAs to PMT) at 875 nm. SAXS Data was collected at beamline 12-ID at Argonne National Laboratory's Advanced Photon Source. The samples were probed using 12 keV (1.033 Å) x-rays, and the sample-to-detector distance was calibrated from a silver behenate standard. The beam was collimated using two sets of slits and a pinhole was used to remove parasitic scattering. The beamwidth was approximately 200 – 300 μm horizontally and 50 μm vertically.

Importantly, samples obtained by annealing the polymer blends between two glass coverslips that were scanned with the X-ray beam perpendicular to the substrate did not yield meaningful data in most systems. This was taken as a strong indication that the samples were all highly aligned in a direction parallel to the substrate—very few samples showed any meaningful data, and then only giving very weak signal, despite the large degree of reflectivity observed in the optical data. This was confirmed by aligning the substrates parallel to the X-ray beam and scanning through the entirety of a sample. In this arrangement, multiple scattering peaks could be observed for most systems. However, due to the small film thickness, scattering from the substrate or glass coverslips was unavoidable and contributed significantly to the background noise. As a result, while the samples clearly had ordered lamellae as confirmed by SEM and optical spectroscopy, not all samples were able to be properly characterized with SAXS, especially samples with large periodicities where the q_0 scattering peak was obscured by the substrate scattering. As a result,

lamellar spacings were not obtainable for all systems and thus some values were instead inferred from the optical data by comparing the photonic band gaps of systems where SAXS data was obtained to the SAXS lamellar spacings.

Methods:

The synthesis and characterization of macromonomers, brush block copolymers, and brush homopolymers was performed as described previously. Polystyrene and polylactic acid homopolymers were synthesized using the same protocols, and the polystyrene homopolymers were synthesized with the same protocol but using methyl α-bromoisobutyrate as an initiator.

Random copolymers were synthesized using a protocol modified from (2). The random copolymers containing vinylbenzyl chloride, methyl methacrylate, and 4-(diphenylphosphino)styrene monomers were synthesized directly, while the random copolymers bearing azide, amine, olefin, and nitrile groups were synthesized via modification of the vinylbenzyl chloride-styrene random copolymer.

To generate the directly synthesized random copolymers, AIBN was first recrystallized from hot methanol, then filtered and placed under vacuum to remove excess solvent. Styrene, vinylbenzyl chloride, and methylmethacrylate were mixed with basic aluminum oxide and stirred for 30 minutes to remove the stablizing agents present in solution that would impede polymerization, then filtered through a glass frit; vinylbenzylchloride was subsequently passed through plugs of basic alumina (typically two purifications were sufficient) to yield a colorless solution. 4-(diphyenylphosphino)styrene was used as a solid powder with no further purification.

In a typical synthesis, styrene (14.85 ml, 1 equiv.), vinylbenzylchloride (4.5 ml, 0.25 equiv.), AIBN (6.75 g, 0.32 equiv.) and THF (54 mL) were combined in a two-necked round

bottom flask fitted with a rubber septum and a condenser column, then degassed with Argon for ~1 hour. The solution was then placed at 65 °C for 1 hour; conversion was kept low in order to prevent monomer drift. The polymer solution was then cooled in an ice bath and dried on a rotary evaporator to remove the THF. The remaining solution was precipitated in methanol 3 times to remove excess monomer, then dried under vacuum. GPC and NMR were used to determine molecular weights and relative monomer fractions within the RCPs.

The azide-bearing RCPs were synthesized by reacting the vinylbenzyl chloride RCP (4.52 g, 1 equiv.) with sodium azide (0.882 g, ~1.5 equiv. per –Cl group) in DMF (75 mL) at room temperature overnight; this sample was purified via three precipitations in methanol. Complete conversion was noted by H NMR in accordance with previous protocols (3). The amine-bearing RCP was synthesized by reacting the azide-RCP (0.519 g, 1 equiv.) with triphenyl phosphine (1.15 g, ~6 equiv.) in a 10:1 mixture of THF and H_2O (30 mL, 3 mL, respectively) at room temperature for 24 hours (4). Purification was performed by extraction from cold ether.

Click chemistry was used to synthesize the olefin- and nitrile-RCPs; the azide RCP (0.268 g, 1 equiv.) was combined with either 4-ethynylbenoznitrile (0.111 g, ~1.5 equiv. per N_3 group) or N-(propargyl)-cis-5-norbornene-exo-2,3-dicarboximide (0.179 g, ~1.5 equiv. per N_3 group, synthesized using protocols described previously (1)), and with CuBr (35 mg, ~0.4 equiv.), and PMDETA (50 µL, ~0.4 equiv.). This mixture was then dissolved in ~15 mL degassed THF, and the solution was further degassed for ~15 minutes, then placed at 65 °C overnight. The reaction mixture was purified by filtering through a basic alumina column followed by two rounds of precipitation in methanol. For all of the above polymers, molecular weights were confirmed using GPC, and complete conversion of the starting material was observed via shift of the H NMR peak corresponding to the protons geminal to the chloride/azide/amine/"clicked" triazole groups.

Blends were prepared by dissolving BBCPs and HPs in benzene to generate stock solutions at known concentrations. These solutions were then mixed in 20 ml scintillations vials at appropriate concentrations and flash frozen via submersion in liquid nitrogen. Once the samples were fully frozen, they were placed in a vacuum chamber and pumped down to ~200 mbar, then allowed to heat up to room temperature overnight, resulting in fluffy white powders that were a homogenous mixtures of all polymer components.

Lamellar arrays of BBCPs were synthesized by placing the powdered blends in between two substrates (glass slides for reflection and SEM measurements, a Si wafer and a glass coverslip sandwiched between two glass slides for SAXS and IR) and compressed with clamps. Samples were annealed by placing them in a 140 °C oven under vacuum overnight, then allowing them to cool in air. For reflection measurements, the glass slides were left intact—some measurements were also performed by separating the two glass slides sandwiching the polymer and measuring reflectance from the polymer film on a single glass slide, but no difference was noted in the photonic band gap λ_{Max}. Glass slides coated in polymer films that were characterized with SEM were first fractured to expose a polymer surface perpendicular to the glass slides, then stained with fresh RuO_4 vapor for ~ 8 minutes and coated with ~10 nm of amorphous carbon to allow for SEM contrast and to prevent charging, respectively. Samples prepared on Si wafers for SAXS and IR were separated from the coverslip prior to taking measurements.

Modeling Information

Self-Consistent Field Theory (SCFT) was utilized to model systems with bottle brush copolymers by extending the grafted copolymer melt model (5) with a multi-species exchange model (Düchs, Delaney and Fredrickson, to be submitted). A polynorbornene backbone (A) is

grafted evenly with constant grafting density by PS side-arms (B) and PLA side-arms (C). The grafting density is defined as $\tau_{k+l}/(k+l)$ where k is the number of B arms and l is the number of C arms. The position of each grafted arm, τ_j can be calculated from Wang et al (Langmuir 2009, 25(8), 4735–4742) as:

$$\tau_j = \tau_0 + \frac{(j-1)(1-\tau_1)}{k+l} \quad 1 \le j \le k+l$$

The detail formalism of SCFT for bottle brush copolymer + homopolymer blends can be found from Kim et al (to be published).

To match the experimental conditions, $\chi_{BC}N$ is 12.0, as calculated from the length of homopolymer PS and PLA, and χ and N (the degree of polymerization) are calculated from Zalusky et al (6). Additionally, $\chi_{AB}N = \chi_{AC}N = 0$, where the segregation strength of the polynorbornene backbone and all other sidearms are effectively shielded by the high grafting density. This parameterization represents a bottle brush copolymer of PS and PLA grafted arms with molecular weight equal to 987 kg /mol when the backbone length α_A is set to 2.8 and the number of grafted brushes is 140 each of PS and PLA arms. From this parameter setup, the period of lamellar morphology in the bulk is calculated in R_g units, where $1R_g = 7.1$ nm.

Supplementary Data:

List of Polymer Information

MM ID	MW (g/mol)	PDI	DP
PLA-MM	3100	1.113	40
PS-MM	3500	1.019	31

Table S1: Macromonomer Physical Data

BBCP ID	MW (g/mol)	PDI	f_{PS}/f_{PLA}	DP_{PS}	DP_{PLA}
A	987000	1.024	52/48	155	143
B	1406000	1.010	51/49	217	209
C	1517000	1.015	50/50	230	230
D	1763000	1.019	50/50	267	267
E	2110000	1.038	50/50	320	320
F	2648000	1.051	50/50	401	401
G	3035000	1.053	51/50	460	460

Table S2: Brush Block Copolymer Physical Data

HP ID	MW (g/mol)	PDI	DP
PS-3k	3200	1.056	42
PS-6k	6200	1.037	83
PS-12k	12400	1.038	169
Brush PS	139000	1.003	45
PLA-3k	3100	1.286	27
PLA-6k	6700	1.244	62
PLA-12k	13900	1.396	133
Brush PLA	151000	1.006	43

Table S3: Homopolymer Physical Data

RCP ID	MW (g/mol)	PDI	$f_{P\text{-}X}$	DP
P-S-VBzCl	5200	1.163	24.4	45
P-S-N_3	5770	1.140	24.0	44
P-S-NB	8010	1.199	18.2	56
P-S-CN	7140	1.144	26.9	46
P-S-NH_2	6500	1.154	7.7	50
P-S-MMA	5210	1.115	29.6	52
P-S-PPh_3	6520	1.508	16.9	49

Table S4: Random Copolymer Physical Data

Brush Block Copolymer Blend Photonic Band Gap and Lamellar Spacing Data

*d_{Lam} for each sample was calculated using small angle X-ray scattering. Values noted with a star could not be measured directly and thus were interpolated based upon the photonic band gap position and the directly measured d_{Lam} values for other BBCP blends.

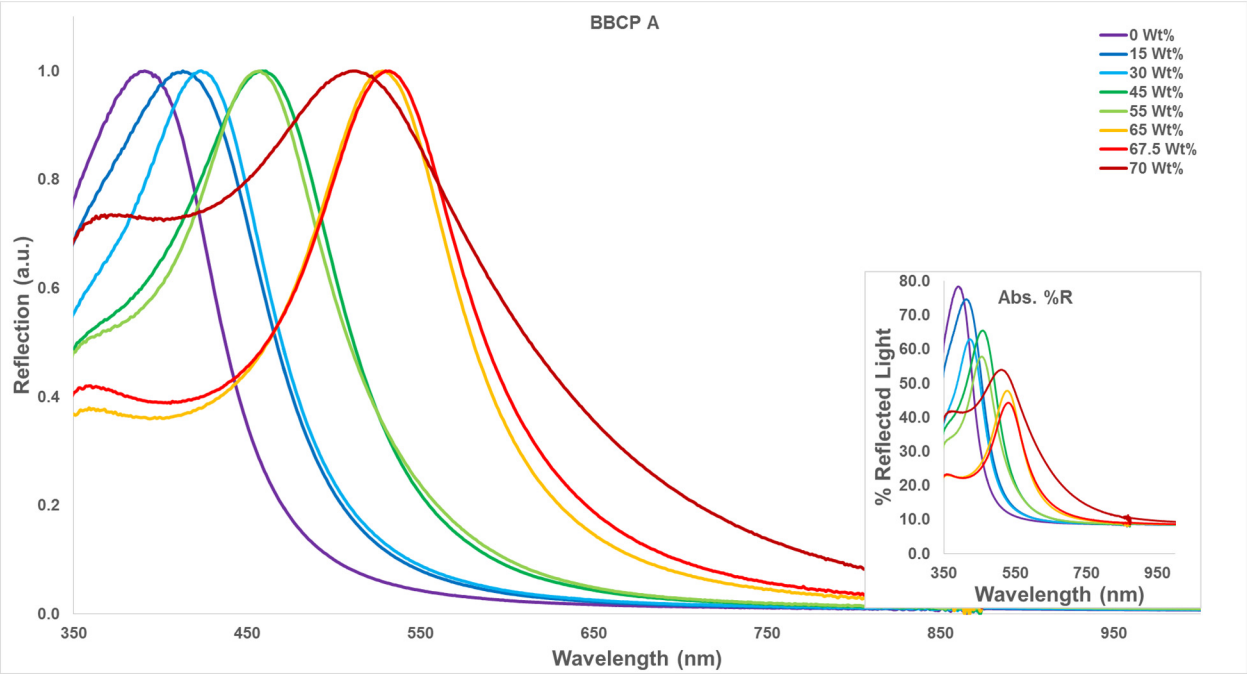

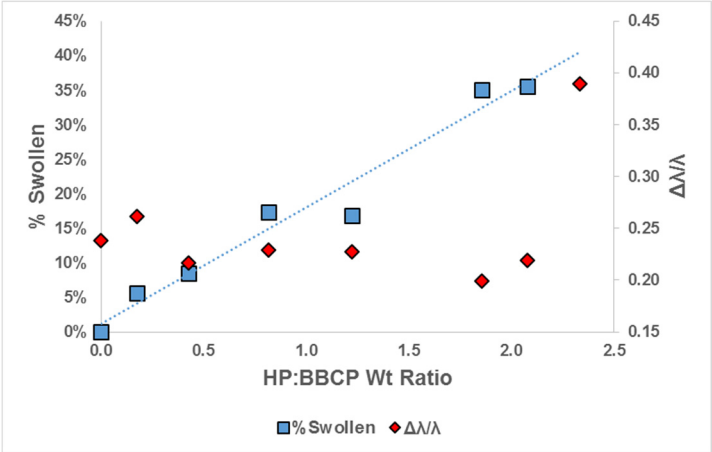

BBCP ID	Wt% HP	λ_{Max} (nm)	d_{Lam} (nm)	%Swollen	Δλ/λ
A	0.0%	391	128	-	0.238
A	15.0%	413	134	5.63%	0.262
A	30.0%	424	141*	8.44%	0.217
A	45.0%	459	156	17.4%	0.229
A	55.0%	457	171	16.9%	0.228
A	65.0%	528	188	35.0%	0.199
A	67.5%	530	197	35.5%	0.219
A	70.0%	513	191	31.2%	0.390

Figure S1: Brush Block Copolymer A Blend Information

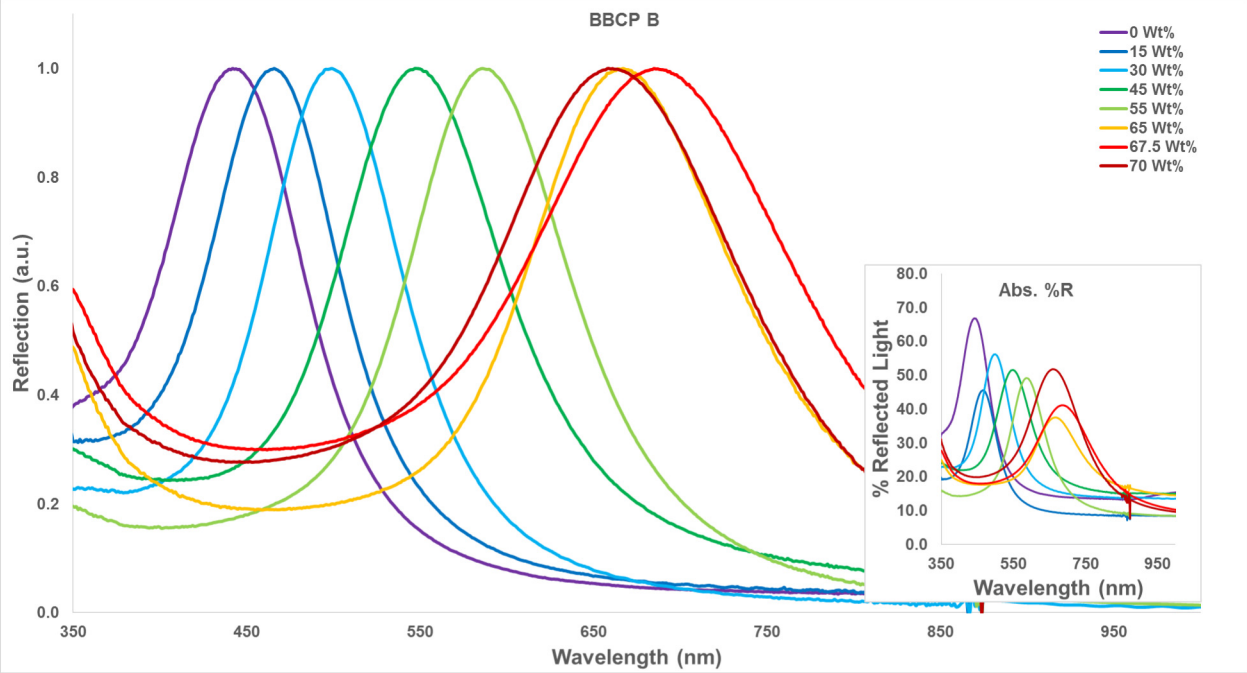

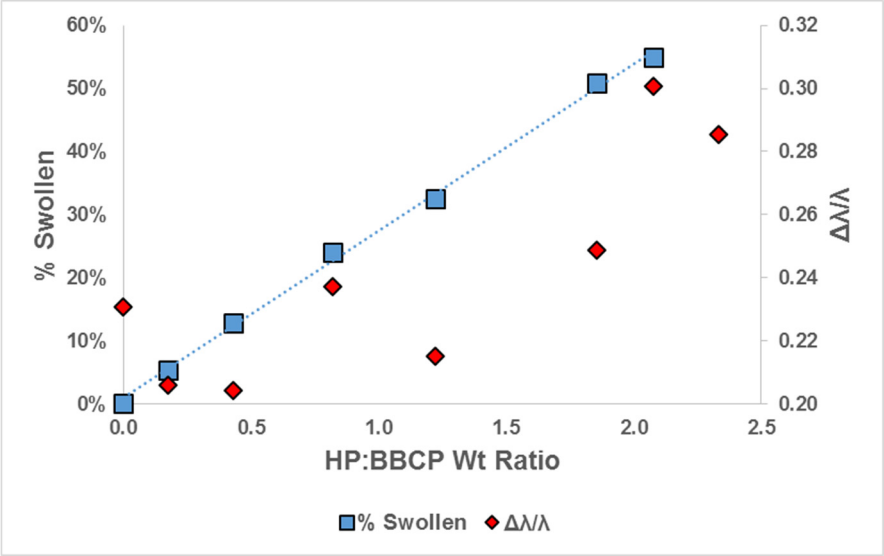

BBCP ID	Wt% HP	λ_{Max} (nm)	d_{Lam} (nm)	%Swollen	Δλ/λ
B	0.0%	442	143	-	0.231
B	15.0%	466	152	5.43%	0.206
B	30.0%	499	164	12.9%	0.204
B	45.0%	548	177	24.0%	0.237
B	55.0%	586	194	32.6%	0.215
B	65.0%	667	221*	50.9%	0.249
B	67.5%	685	227*	55.0%	0.301
B	70.0%	659	219*	49.1%	0.285

Figure S2: Brush Block Copolymer B Blend Information

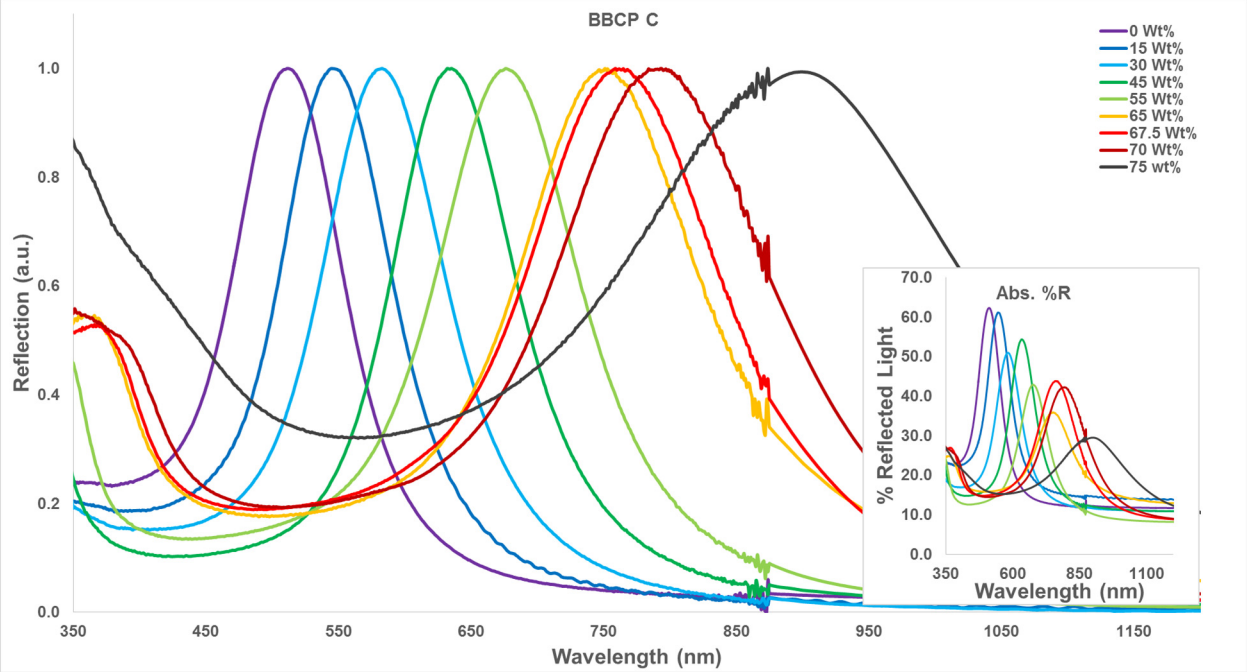

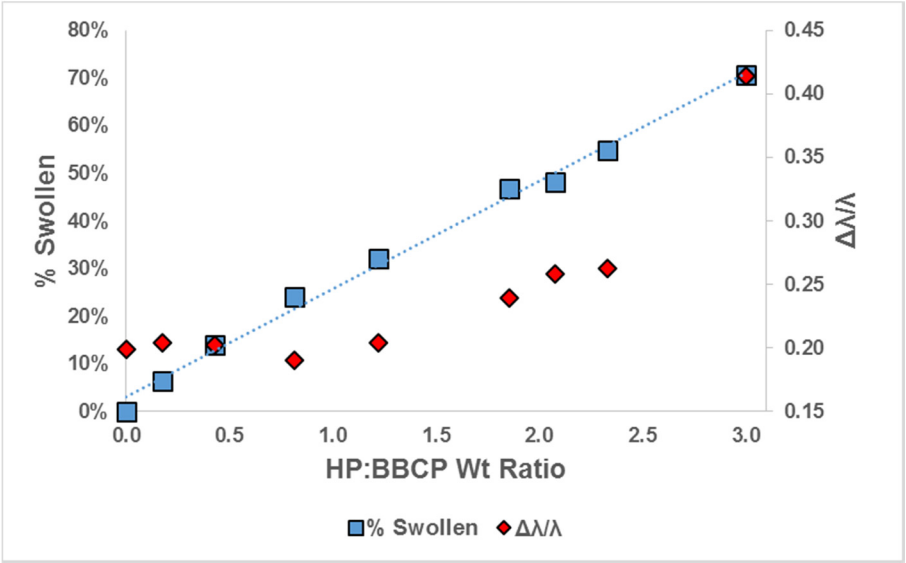

BBCP ID	Wt% HP	λ_{Max} (nm)	d_{Lam} (nm)	%Swollen	Δλ/λ
C	0.0%	512	170*	-	0.199
C	15.0%	545	181*	6.45%	0.204
C	30.0%	583	195	13.9%	0.202
C	45.0%	635	205	24.0%	0.191
C	55.0%	676	222	32.0%	0.204
C	65.0%	751	242	46.7%	0.240
C	67.5%	759	251*	48.2%	0.258
C	70.0%	793	263*	54.9%	0.262
C	75.0%	874	290*	70.7%	0.414

Figure S3: Brush Block Copolymer C Blend Information

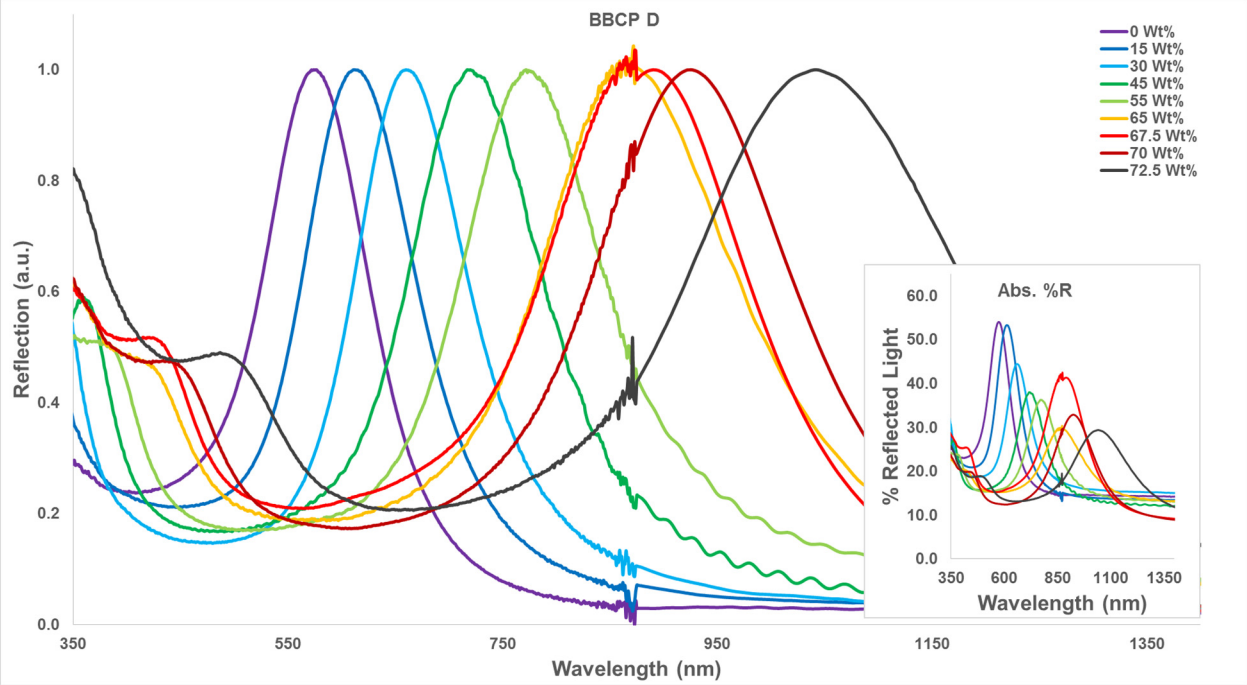

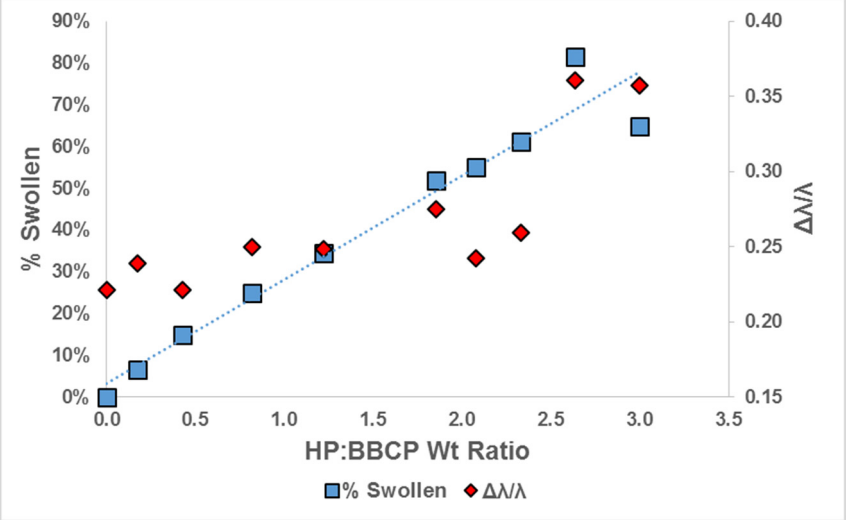

BBCP ID	Wt% HP	λ_{Max} (nm)	d_{Lam} (nm)	%Swollen	Δλ/λ
D	0.0%	574	195	-	0.221
D	15.0%	611	203*	6.45%	0.239
D	30.0%	660	216	15.0%	0.221
D	45.0%	717	230	24.9%	0.250
D	55.0%	772	254	34.5%	0.249
D	65.0%	872	270	51.9%	0.275
D	67.5%	890	295*	55.1%	0.243
D	70.0%	925	307*	61.1%	0.259
D	72.5%	1042	346*	81.5%	0.361
D	75.0%	946	314*	64.8%	0.357

Figure S4: Brush Block Copolymer D Blend Information

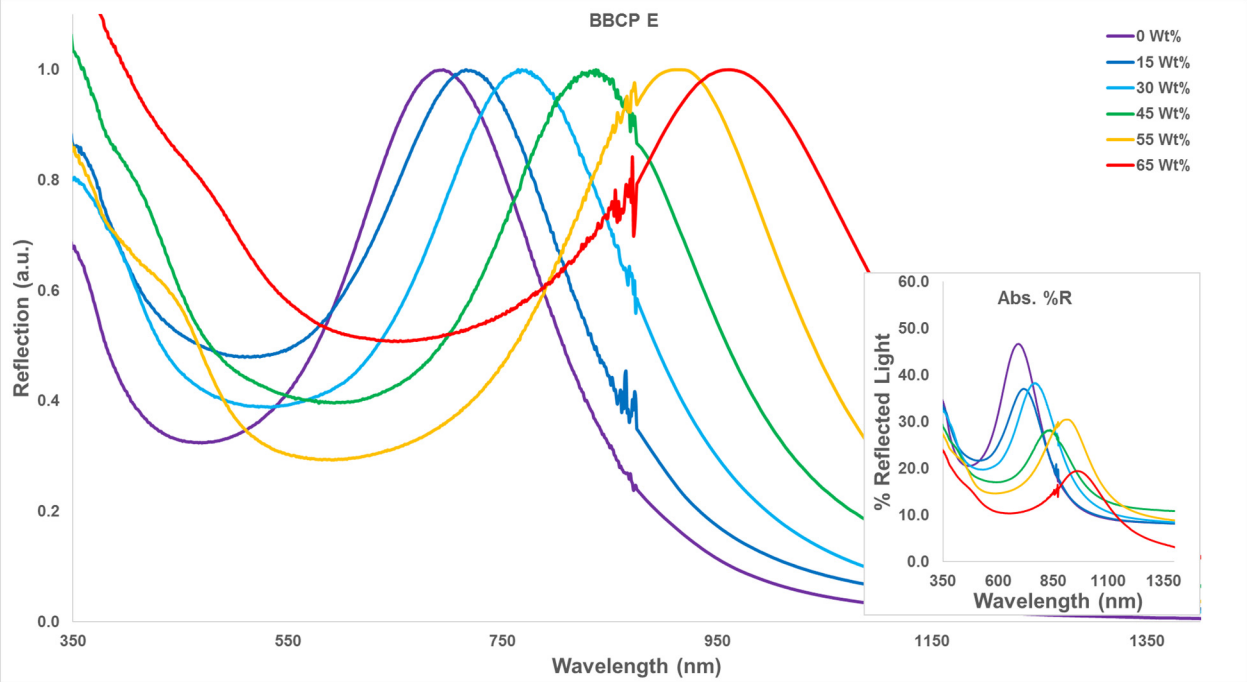

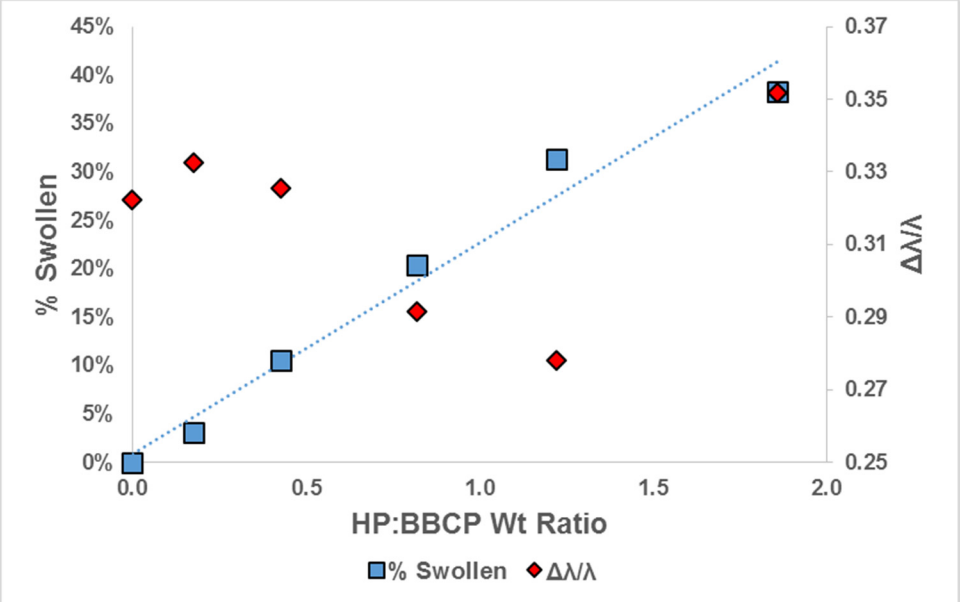

BBCP ID	Wt% HP	λ_{Max} (nm)	d_{Lam} (nm)	%Swollen	ΔλΛ/λ
E	0.0%	695	227	-	0.322
E	15.0%	716	237*	3.02%	0.332
E	30.0%	768	250	10.5%	0.326
E	45.0%	837	267	20.4%	0.292
E	55.0%	913	284	31.4%	0.278
E	65.0%	961	309	38.3%	0.352

Figure S5: Brush Block Copolymer E Blend Information

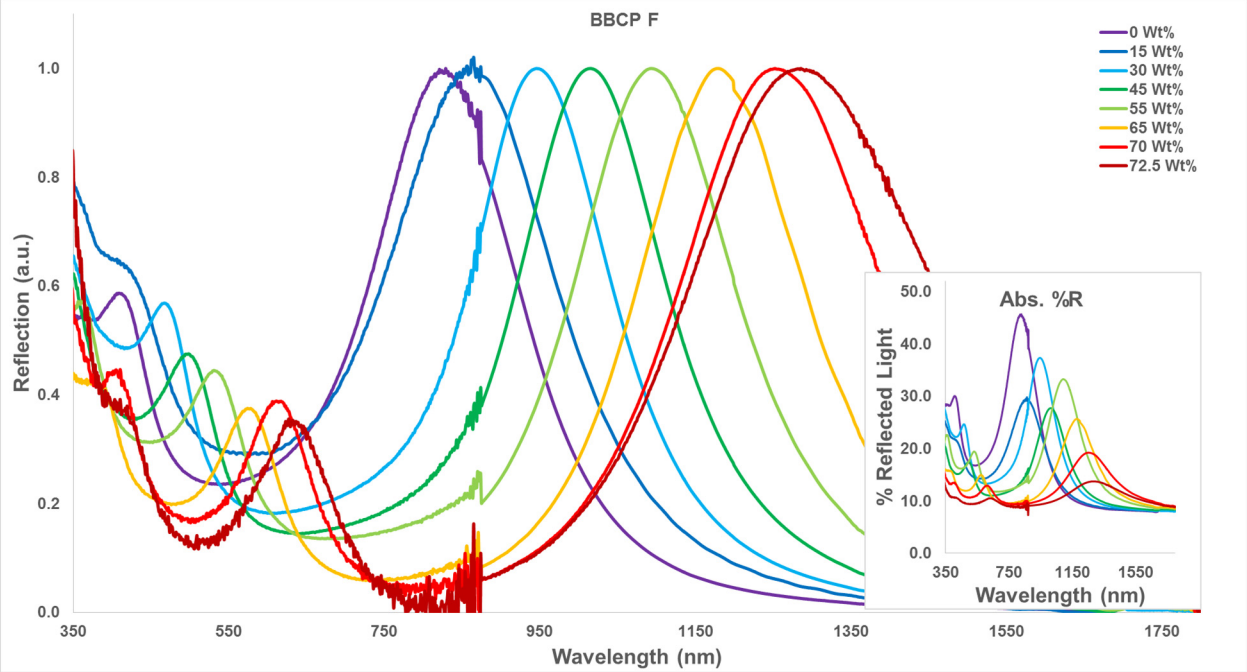

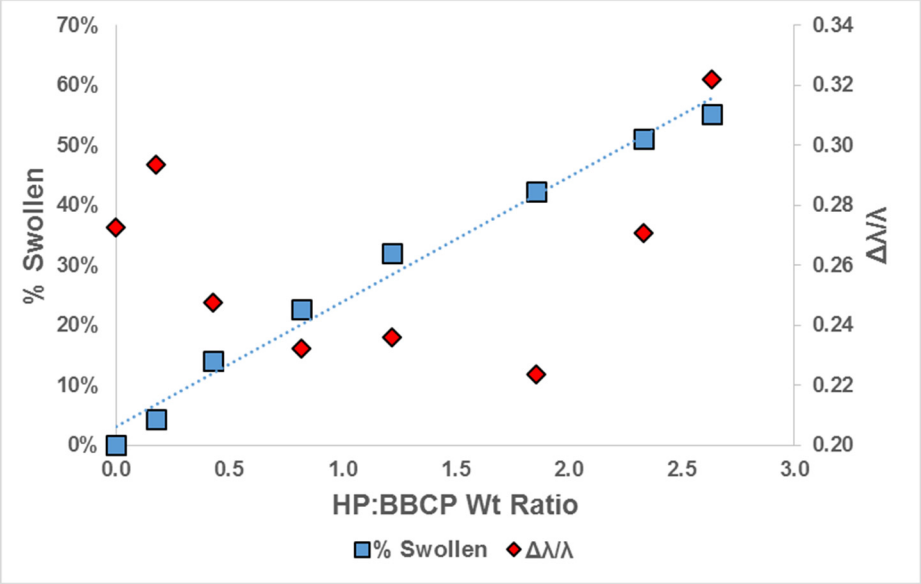

BBCP ID	Wt% HP	λ_{Max} (nm)	d_{Lam} (nm)	%Swollen	ΔλΛ
F	0.0%	829	275*	-	0.273
F	15.0%	865	287*	4.34%	0.294
F	30.0%	946	314*	14.1%	0.247
F	45.0%	1016	340	22.6%	0.232
F	55.0%	1094	362	32.0%	0.236
F	65.0%	1180	391*	42.3%	0.224
F	70.0%	1253	416*	51.1%	0.271
F	72.5%	1286	426*	55.1%	0.322

Figure S6: Brush Block Copolymer F Blend Information

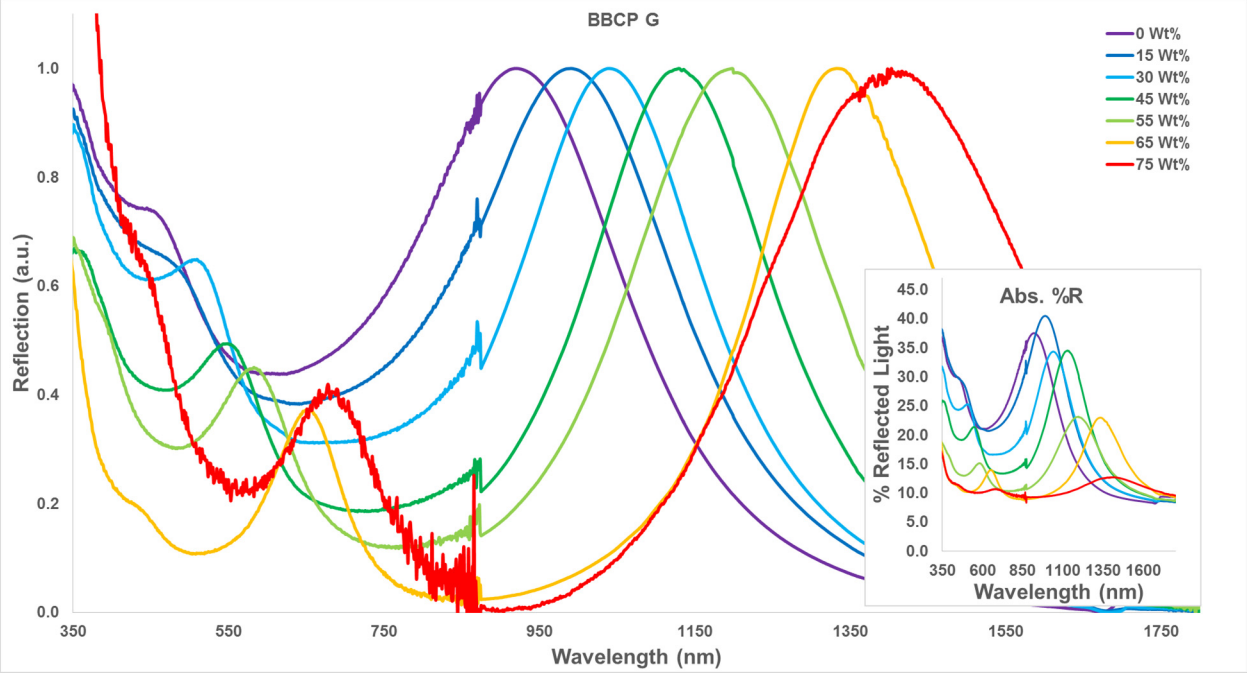

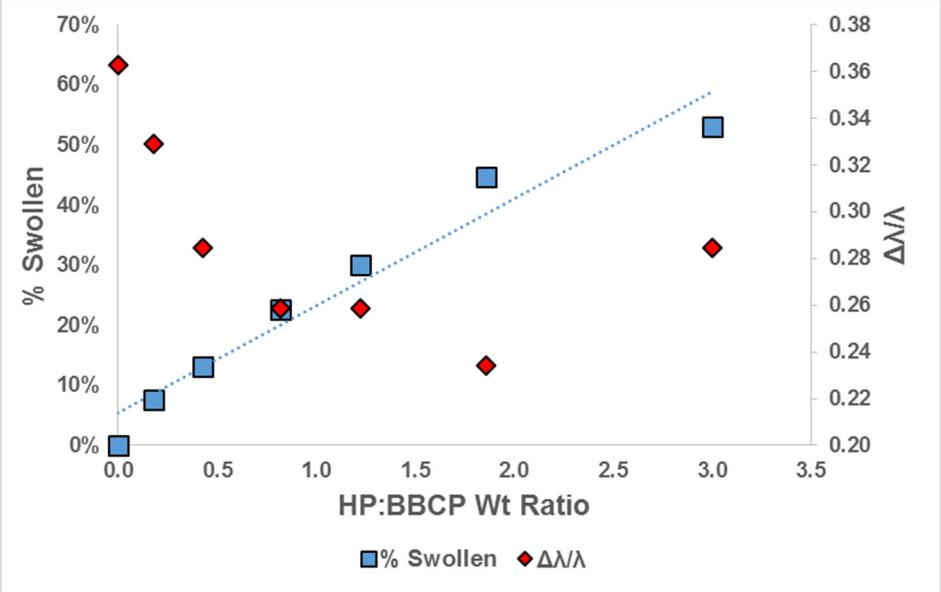

BBCP ID	Wt% HP	λ_{Max} (nm)	d_{Lam} (nm)	%Swollen	ΔΛ/Λ
G	0.0%	921	305*	-	0.363
G	15.0%	991	329*	7.60%	0.329
G	30.0%	1041	345*	13.0%	0.284
G	45.0%	1130	374*	22.7%	0.258
G	55.0%	1198	397*	30.1%	0.259
G	65.0%	1333	442*	44.7%	0.234
G	75.0%	1403	485*	52.3%	0.285

Figure S7: Brush Block Copolymer G Blend Information

Images of BBCP Homopolymer Blends

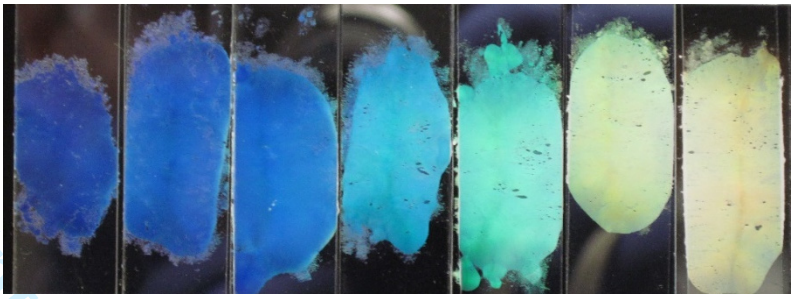

Figure S8: Photos of BBCP A Blends (from left, 0%, 15%, 30%, 45%, 55%, 65%, 67.5%)

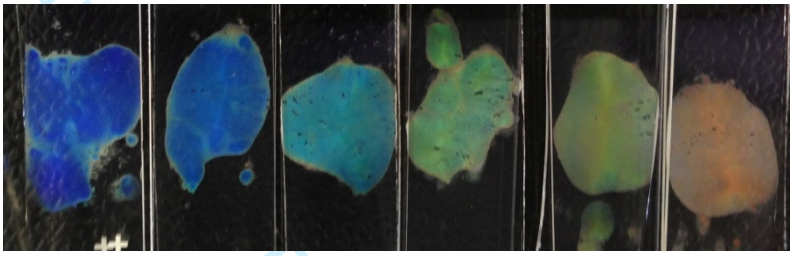

Figure S9: Photos of BBCP B Blends (from left, 0%, 15%, 30%, 45%, 55%, 65%)

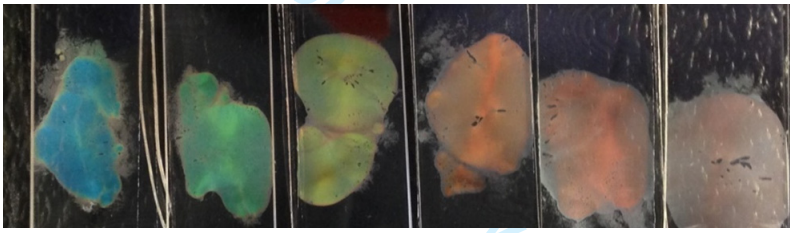

Figure S10: Photos of BBCP C Blends (from left, 0%, 15%, 30%, 45%, 55%, 65%)

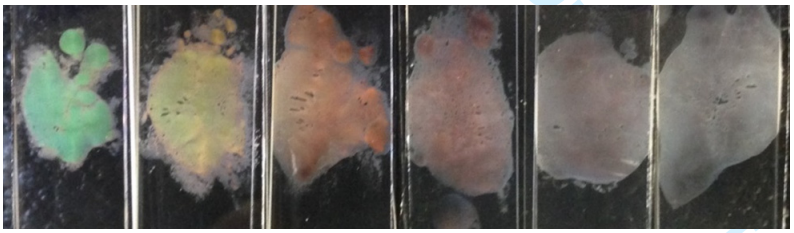

Figure S11: Photos of BBCP D Blends (from left, 0%, 15%, 30%, 45%, 55%, 65%)

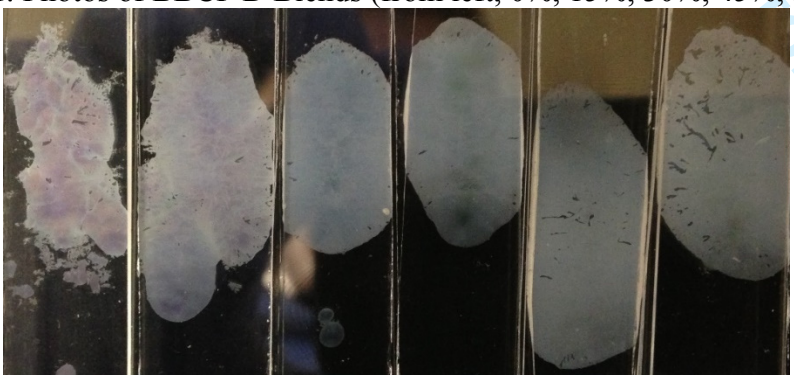

Figure S12: Photos of BBCP F Blends (from left, 0%, 15%, 30%, 45%, 55%, 65%)

UV-Vis data for RCP Blends

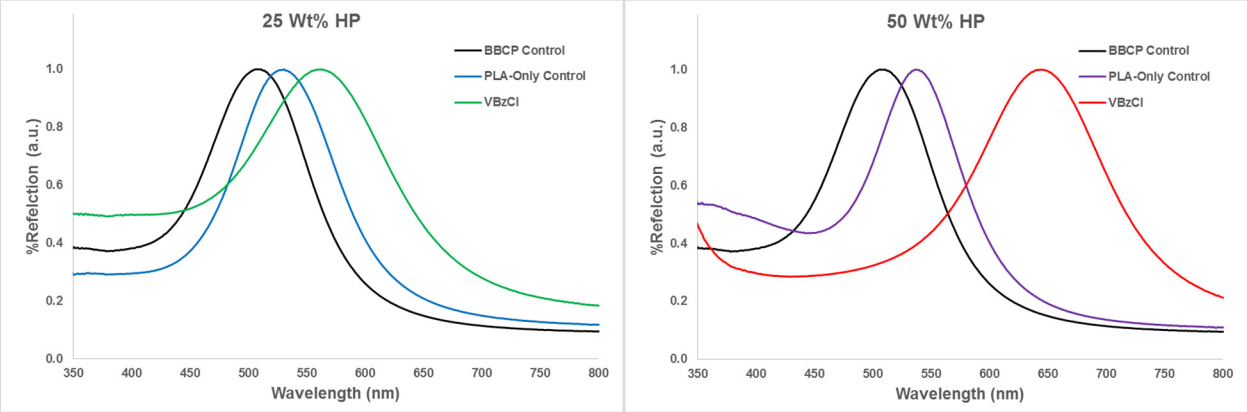

Figure S13: UV-Vis spectra of P-S-VBzCl/BBCP Blends. Note that the total weight % of homopolymer is equal amounts RCP and PLA HP. Samples in which the same amount of PLA HP was added, but the RCP was not added are provided as controls for comparison.

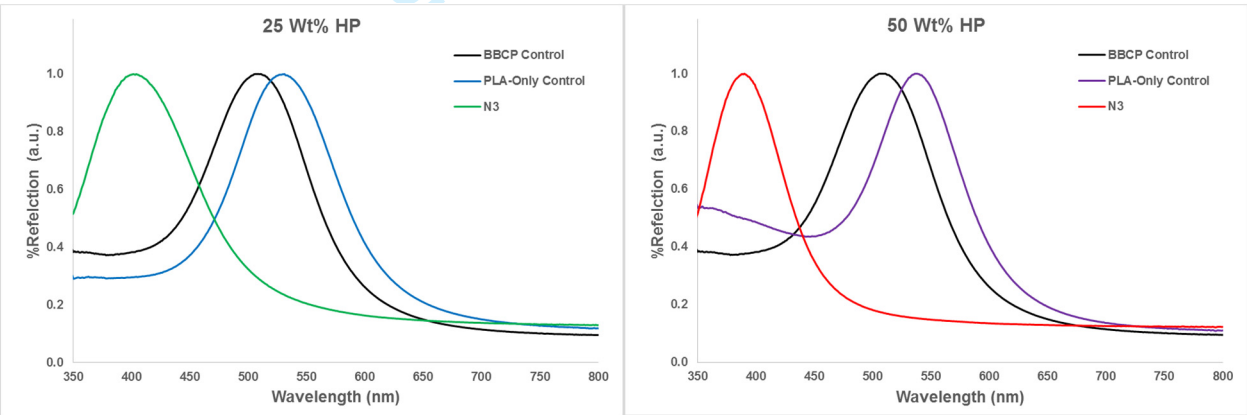

Figure S14: UV-Vis spectra of P-S-N_3/BBCP Blends. Note that the total weight % of homopolymer is equal amounts RCP and PLA HP. Samples in which the same amount of PLA HP was added, but the RCP was not added are provided as controls for comparison.

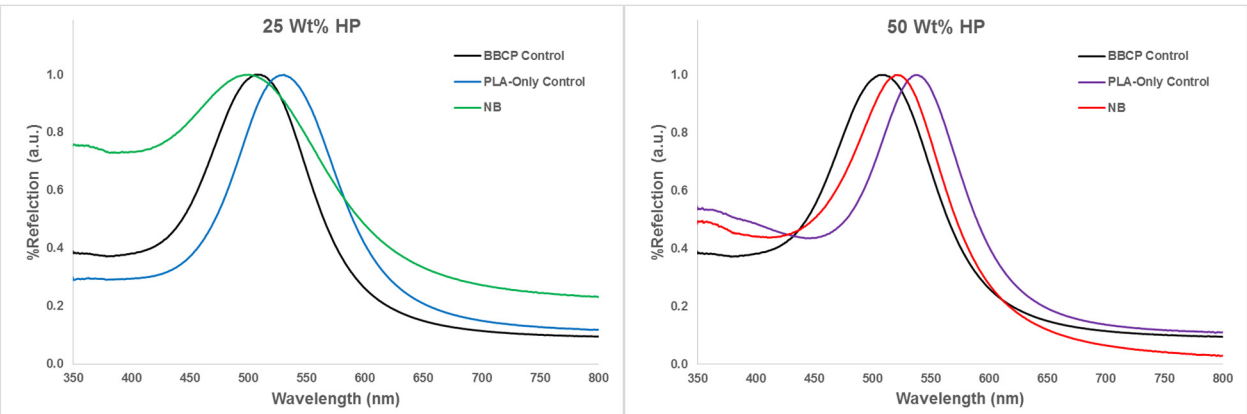

Figure S15: UV-Vis spectra of P-S-Norbornene/BBCP Blends. Note that the total weight % of homopolymer is equal amounts RCP and PLA HP. Samples in which the same amount of PLA HP was added, but the RCP was not added are provided as controls for comparison.

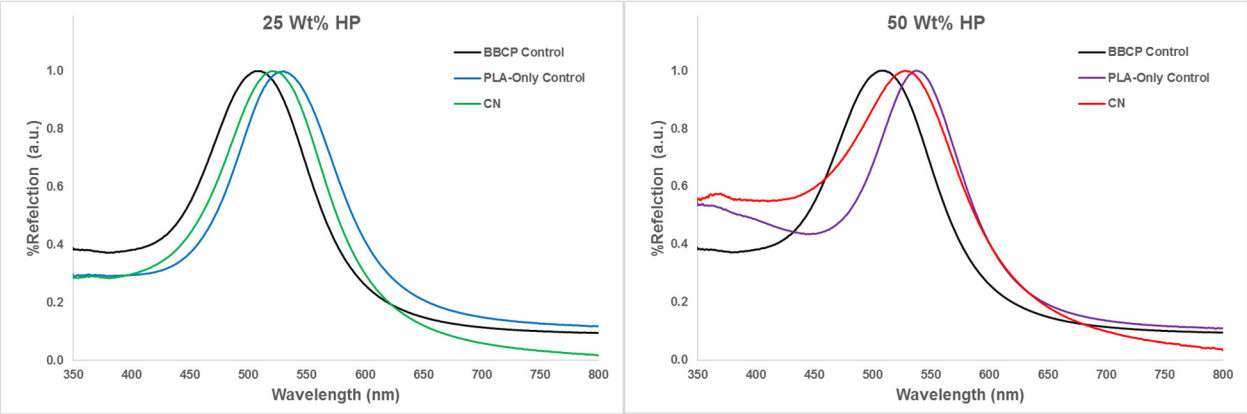

Figure S16: UV-Vis spectra of P-S-Nitrile/BBCP Blends. Note that the total weight % of homopolymer is equal amounts RCP and PLA HP. Samples in which the same amount of PLA HP was added, but the RCP was not are provided as controls for comparison.

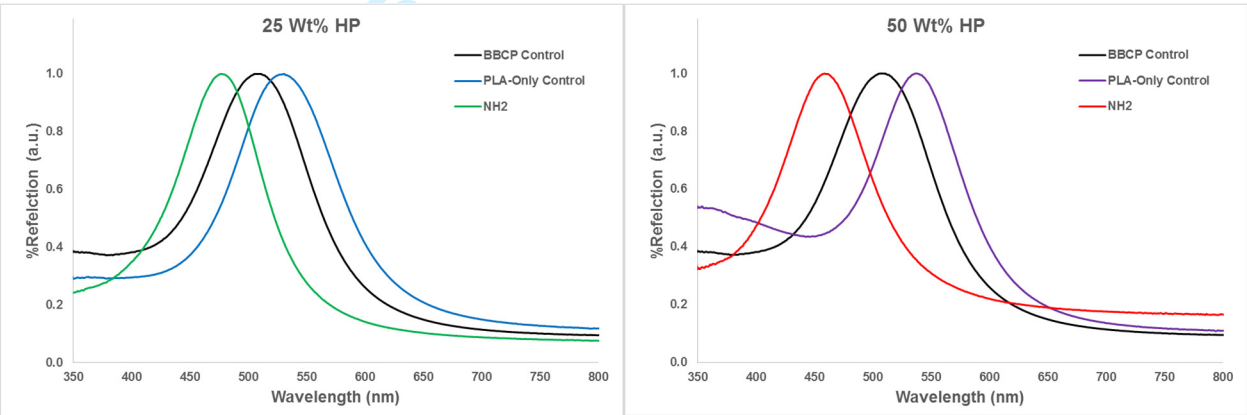

Figure S17: UV-Vis spectra of P-S-NH_2/BBCP Blends. Note that the total weight % of homopolymer is equal amounts RCP and PLA HP. Samples in which the same amount of PLA HP was added, but the RCP was not added are provided as controls for comparison.

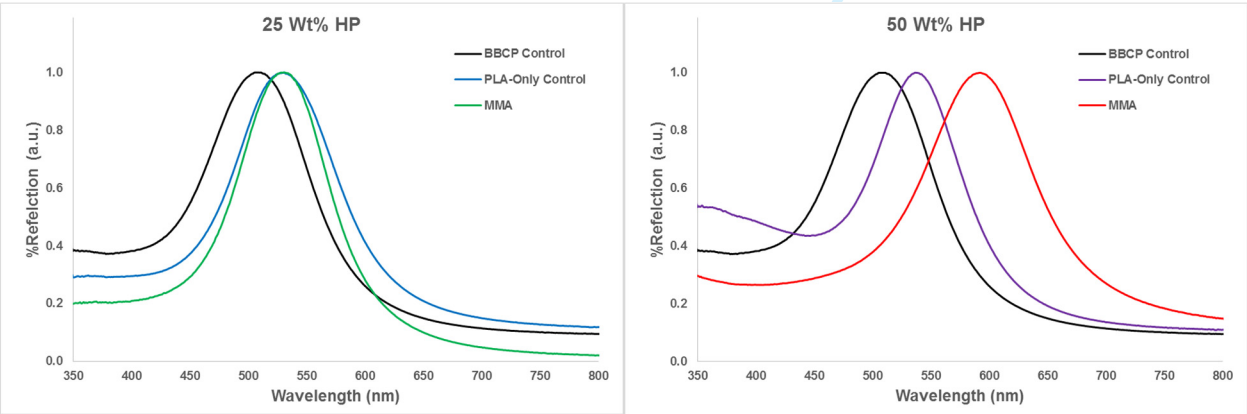

Figure S18: UV-Vis spectra of P-S-MMA/BBCP Blends. Note that the total weight % of homopolymer is equal amounts RCP and PLA HP. Samples in which the same amount of PLA HP was added, but the RCP was not added are provided as controls for comparison.

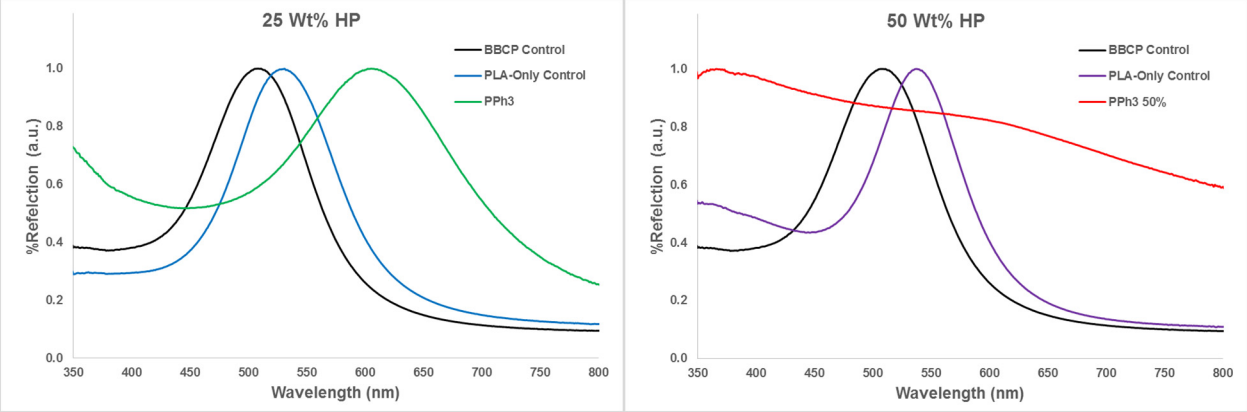

Figure S19: UV-Vis spectra of P-S-PPh_3/BBCP Blends. Note that the total weight % of homopolymer is equal amounts RCP and PLA HP. Samples in which the same amount of PLA HP was added, but the RCP was not added are provided as controls for comparison. No photonic band gap was observed in the sample with 50 wt% PPh_3 HP and PLA HP.

Blend System	Wt% RCP+HP	λ_{Max} (nm)	%Shifted
BBCP C	0.0%	512	-
PLA-Only	14.2%	529	3.32%
PLA-Only	33.3%	527	2.93%
P-S-VBzCl	25.0%	561	9.64%
P-S-VBzCl	50.0%	643	25.6%
P-S-N_3	25.0%	400	-21.9%
P-S-N_3	50.0%	389	-24.0%
P-S-NB	25.0%	494	-3.52%
P-S-NB	50.0%	520	1.56%
P-S-CN	25.0%	523	2.21%
P-S-CN	50.0%	526	2.67%
P-S-NH_2	25.0%	477	-6.84%
P-S-NH_2	50.0%	449	-12.2%
P-S-MMA	25.0%	534	4.36%
P-S-MMA	50.0%	585	14.2%
P-S-PPh_3	25.0%	610	19.2%
P-S-PPh_3	50.0%	-	-

Table S5: Block Copolymer Random Copolymer Blend Information. Note that the PLA-Only blend contained amounts of BBCP and PLA-HP that were equivalent to the other blends; because there was no RCP added, the overall weight percent values are different.

Polymer Blends with Different MW HPs

The effects of changing HP MW on the periodicity were also examined, as it has been shown in linear HP/BCP blends that the altering the weight of the homopolymer added to a blend can effect different amounts of swelling. To this end, BBCPs (MW ~1,406,000 g/mol) were blended with HPs that were 2x and 4x larger (~6,000 g/mol and ~12,000 g/mol, respectively) than the BBCP brushes, as well as PS and PLA homobrush polymers with a MW ~45 times that of the macromolecular brushes (~150,000 g/mol). In these systems, increasing the MW of the HP resulted in a greater change in periodicity with increasing HP wt%, but at the cost of decreased ordering, resulting in poorer quality photonic bandgaps—the significant opacity and lack of a band gap in higher HP wt% films indicates that the blends are no longer capable of forming ordered lamellar arrays.

The modeling data for these systems shows that the larger the HP MW, the greater its segmentation to the regions in the center of the lamellae, inbetween different layers of BBCPs. This greater degree of segregation explains both the larger change in periodicity for heavier HPs (as they contribute more to expansion of the lamellae), as well as the limited tolerance of the BBCP arrays for the heavier HPs before phase segregation occurs.

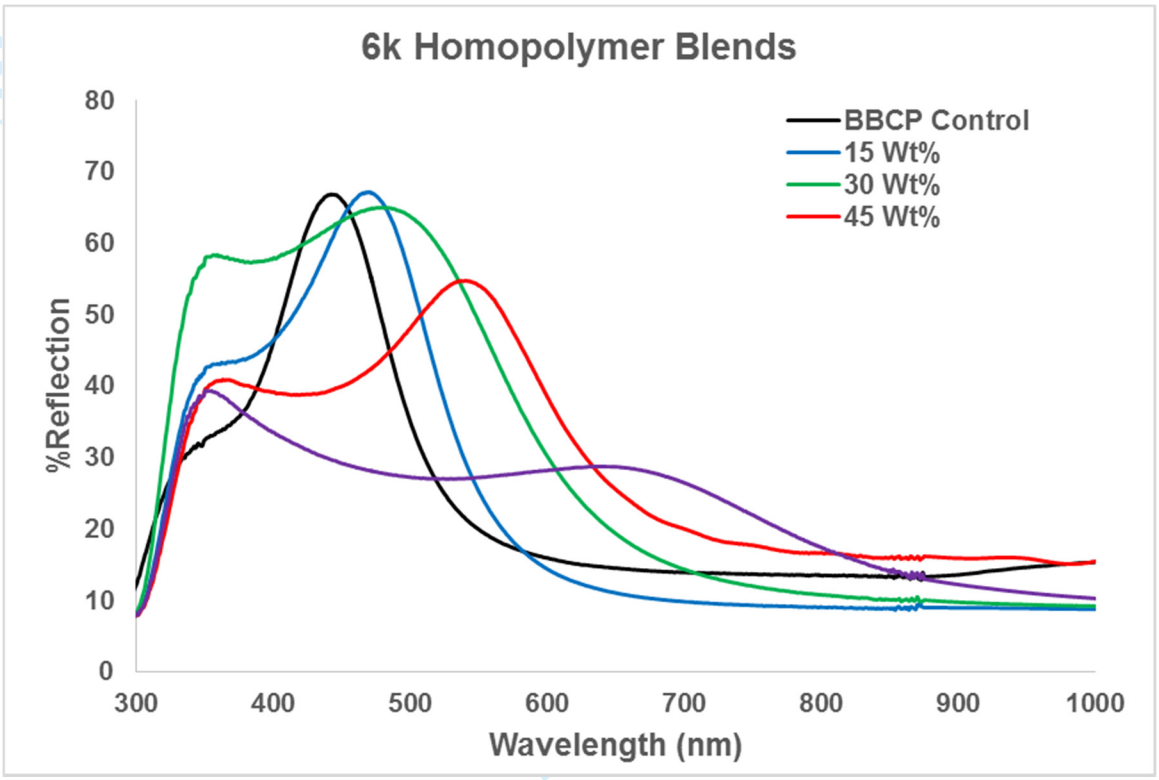

Fig. S20: UV-Vis spectra of BBCP-6k HP Blends.

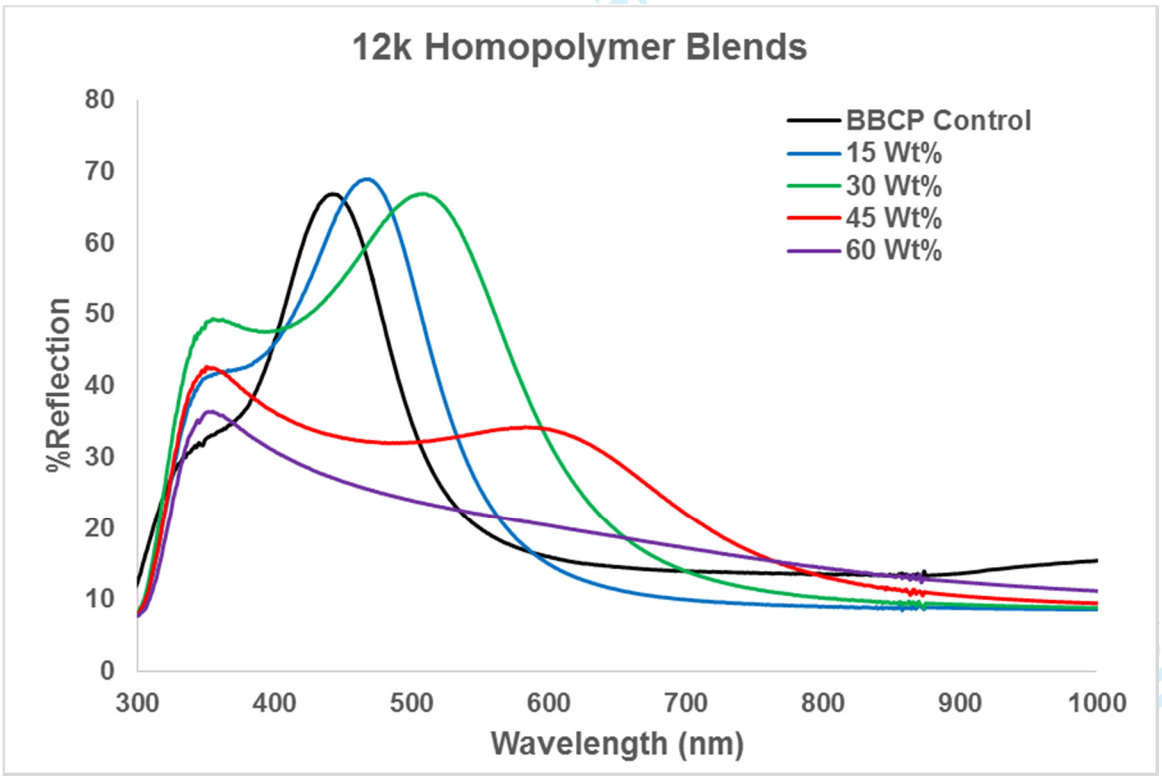

Fig. S21: UV-Vis spectra of BBCP-12k HP Blends.

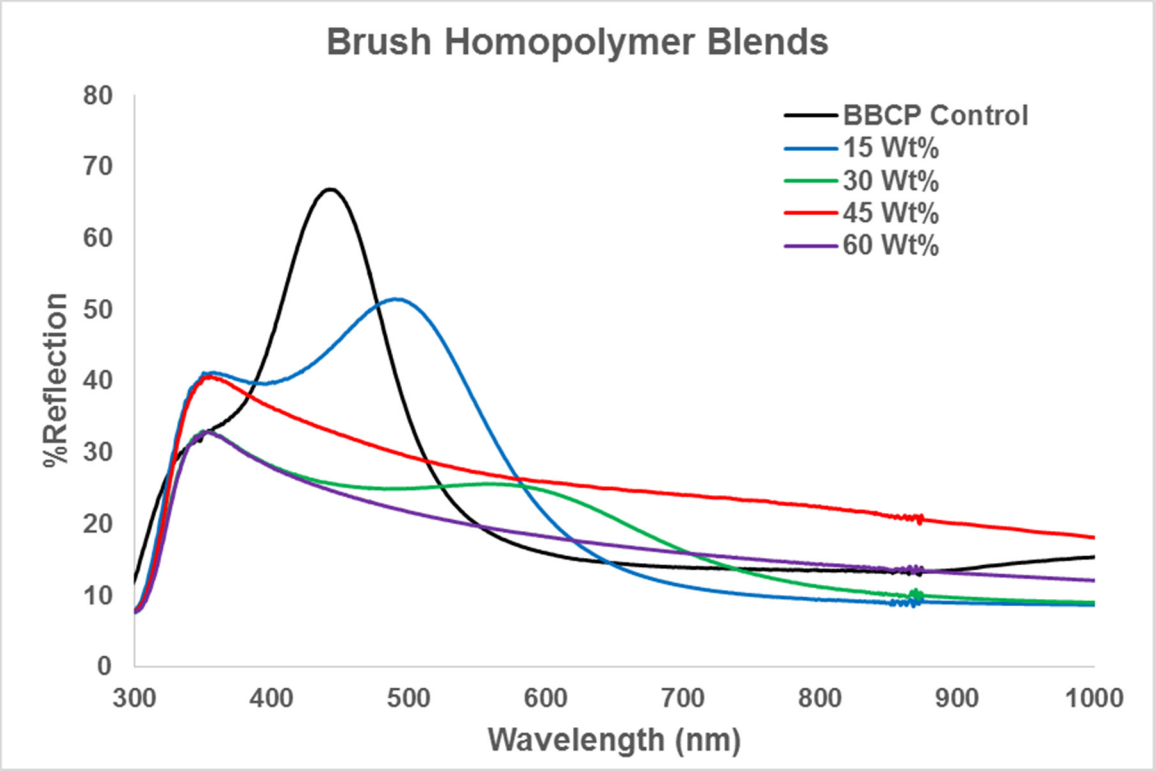

Fig. S22: UV-Vis spectra of BBCP-Brush HP Blends.

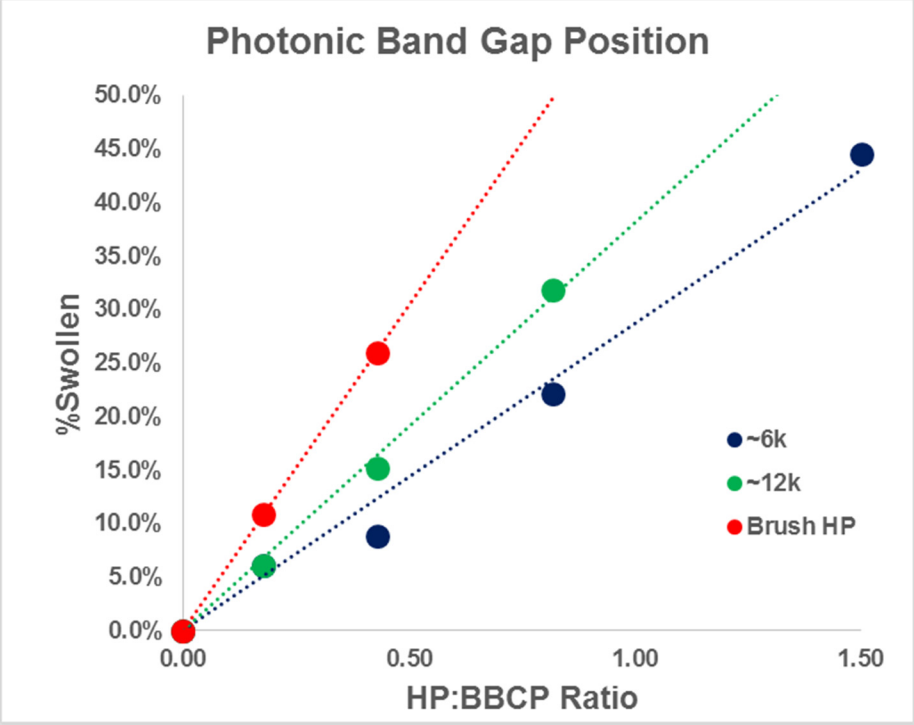

Fig. S23: Photonic band gap position for BBCP/HP blends with different molecular weight HPs.

Additional SEM Data for RCP Blends

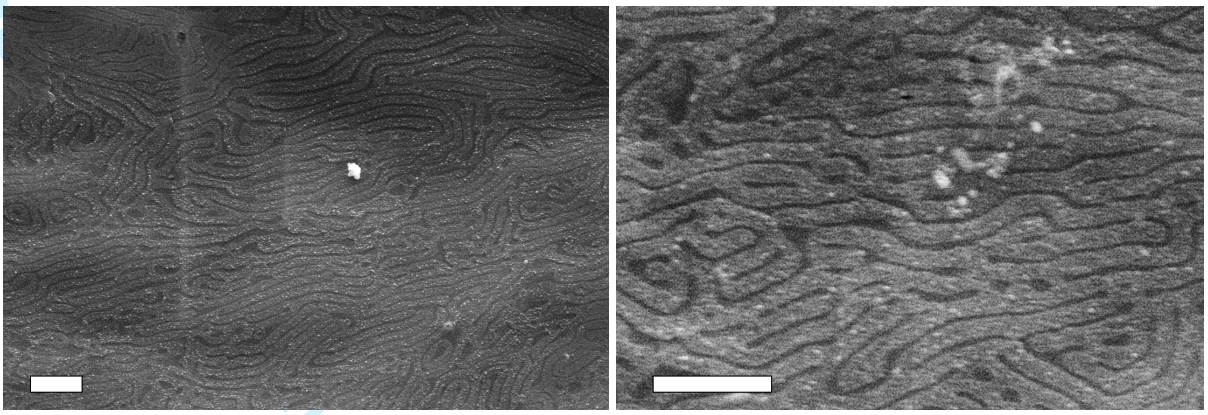

Fig. S24: SEM Images of BBCP/P-S-VBzCl Blends, demonstrating that the structures are lamellar. Scale bars are 1 μm.

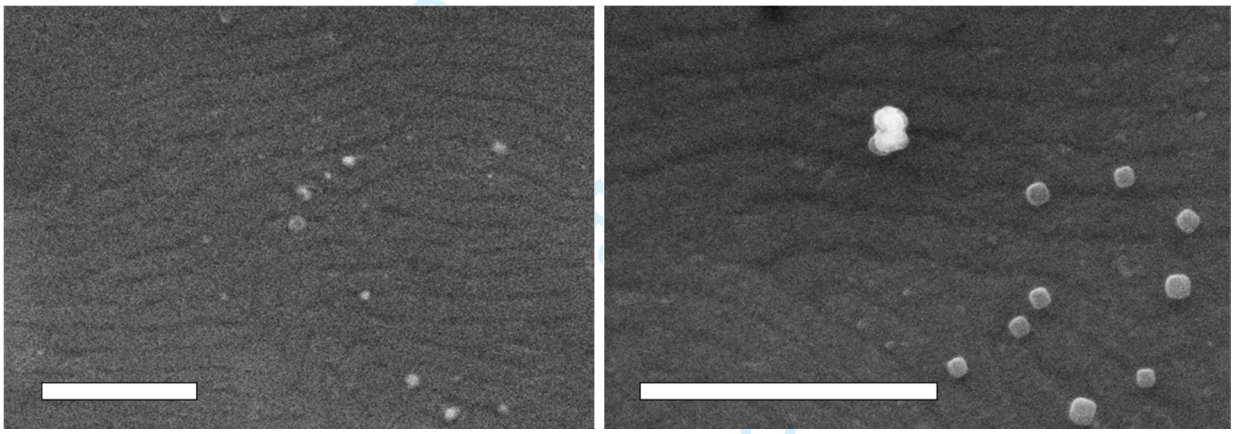

Fig. S25: SEM Images of BBCP/P-S-N_3 Blends, demonstrating that the structures are lamellar. Scale bars are 1 μm.

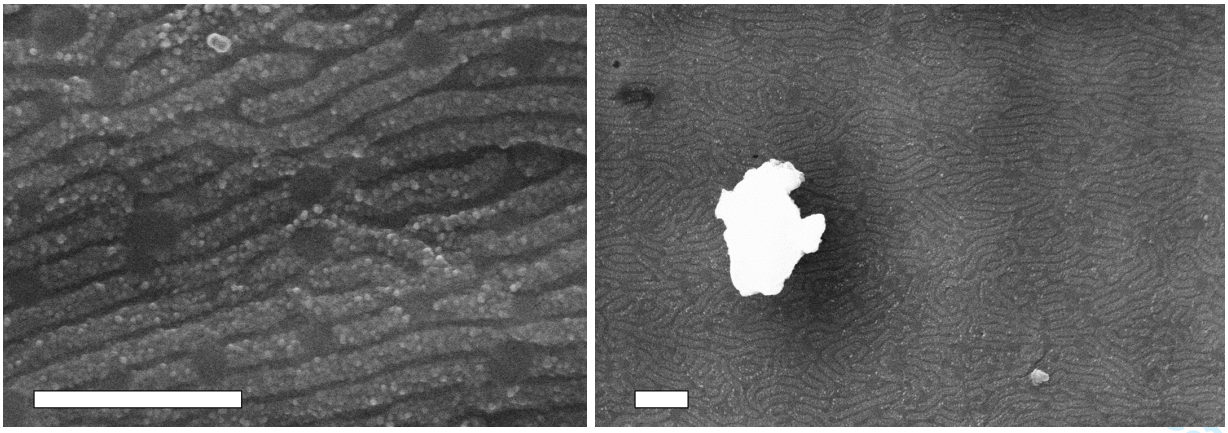

Fig. S26: SEM Images of BBCP/P-S-NB Blends, demonstrating that the structures are lamellar. Scale bars are 1 μm.

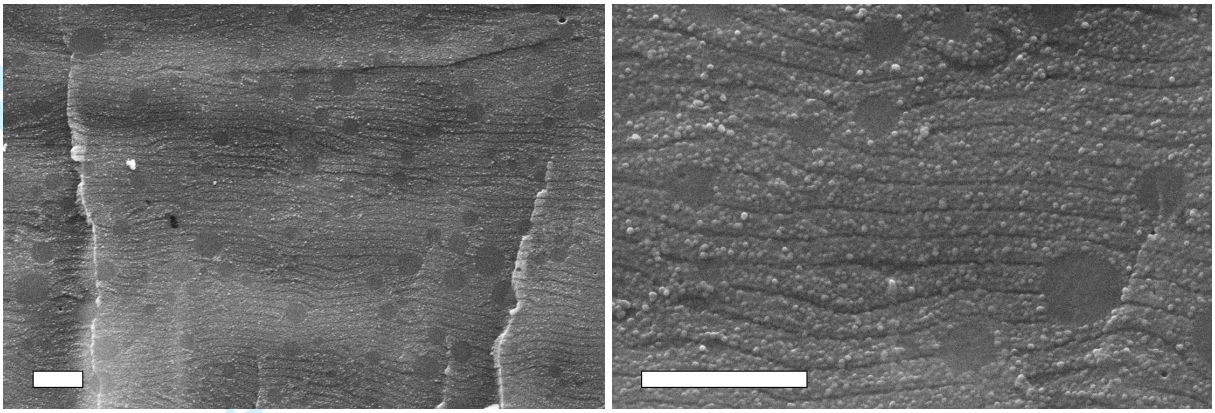

Fig. S27: SEM Images of BBCP/P-S-CN Blends, demonstrating that the structures are lamellar. Scale bars are 1 μm.

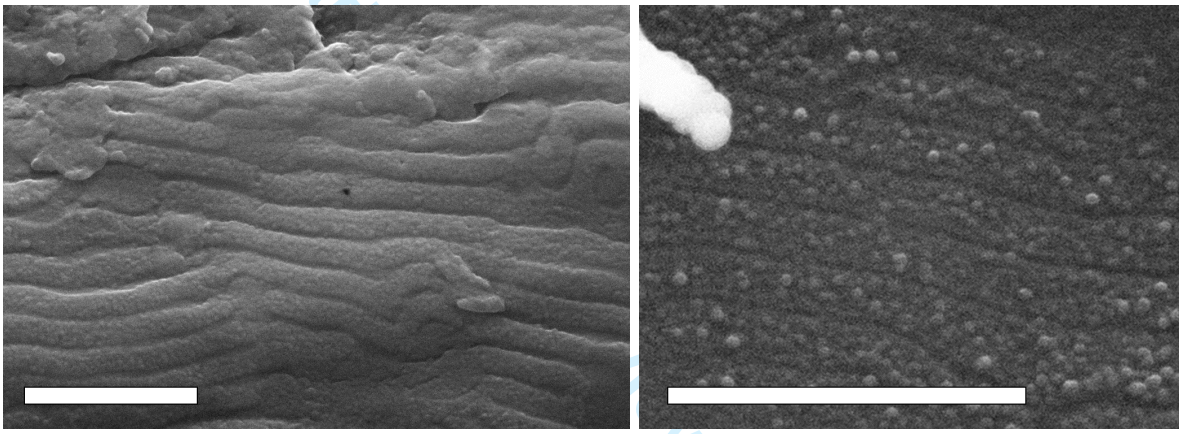

Fig. S28: SEM Images of BBCP/P-S-NH_2 Blends, demonstrating that the structures are lamellar. Scale bars are 1 μm.

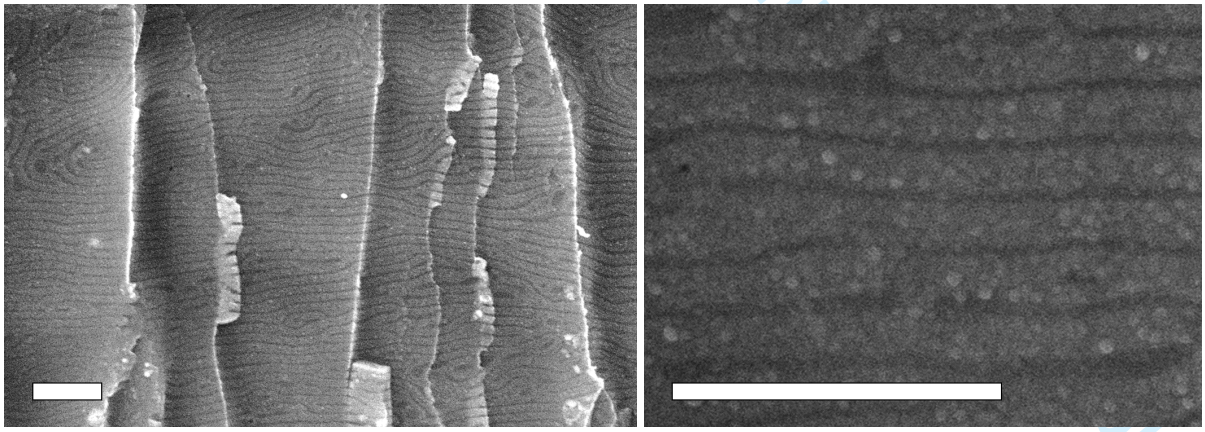

Fig. S29: SEM Images of BBCP/P-S-MMA Blends, demonstrating that the structures are lamellar. Scale bars are 1 μm.

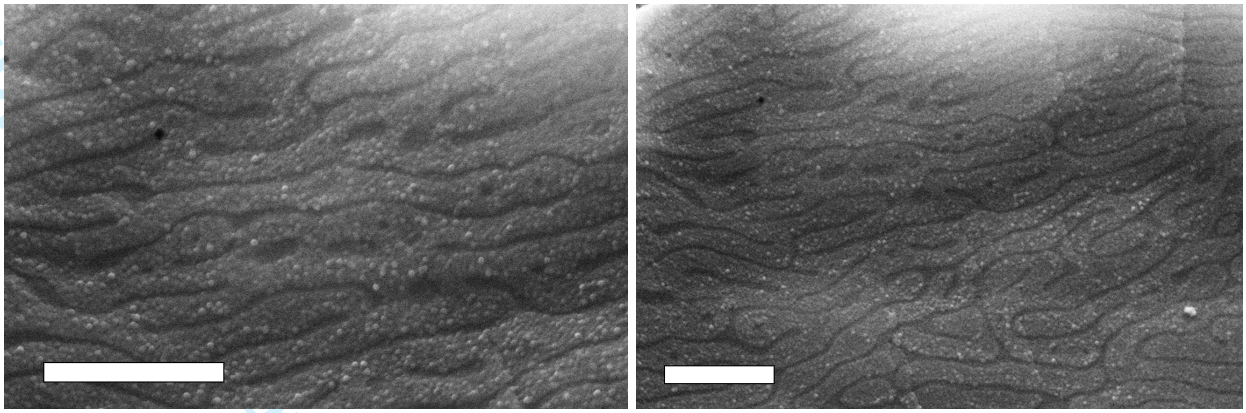

Fig. S30: SEM Images of BBCP/P-S-PPh_3 Blends, demonstrating that the structures are lamellar. Scale bars are 1 μm.

IR Spectra of BBCP-RCP Blends

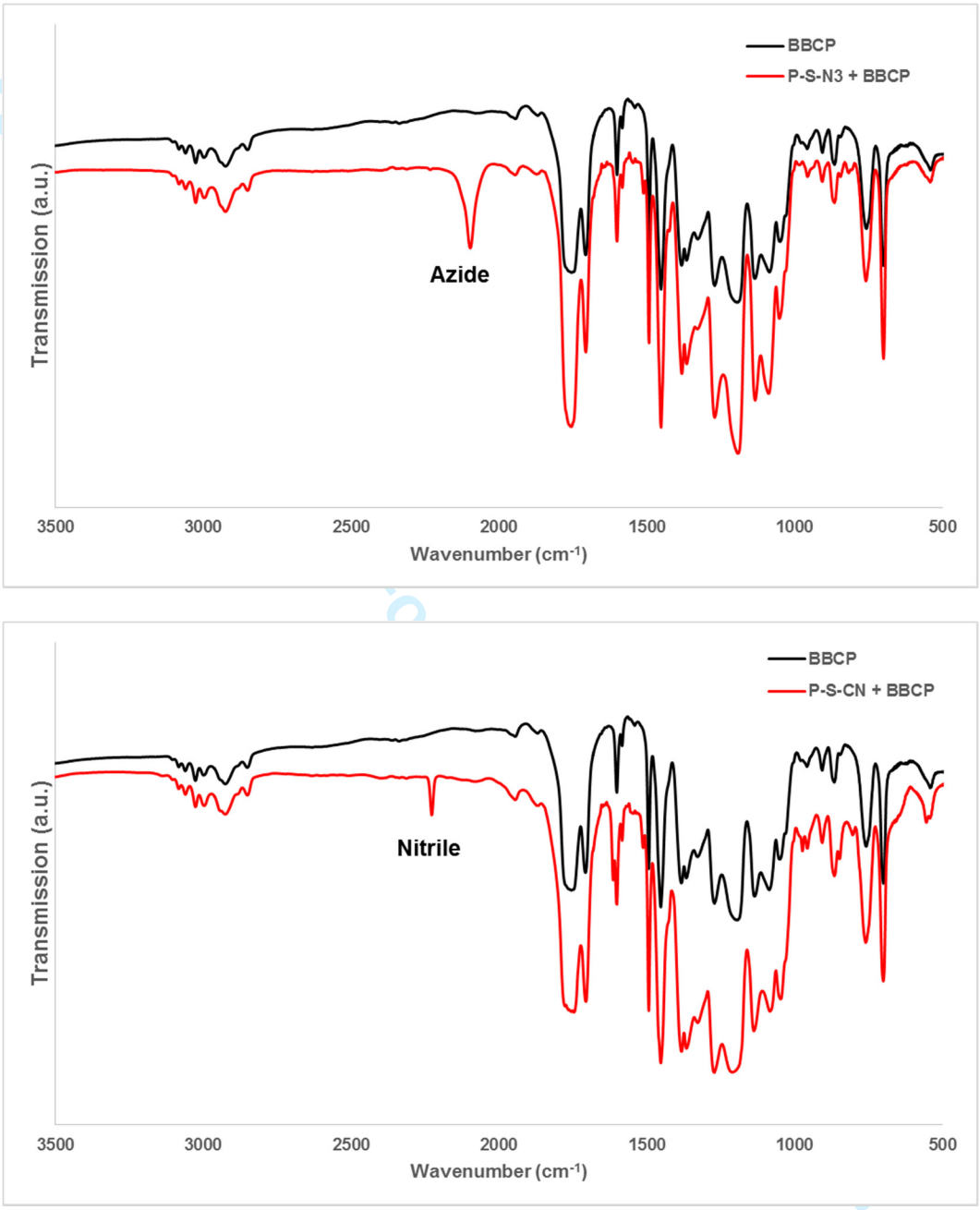

Fig. S31: IR data of unblended polymer films (black traces) and BBCP films with azide- and nitrile-functionalized random copolymers (red traces). Other RCPs were analyzed with IR as well, but the relatively small amount of functional group compared to the BBCPs, as well as the lack of a distinct, unobscured peak that was diagnostic of the RCP in question prevented complete analysis with IR. NMR data (below) was therefore also used to confirm the presence of the additional functional groups.

NMR Data of BBCP-RCP Blends

Because IR data was not able to definitively show evidence of the functional groups in all polymer films, the BBCPs were redissolved in $CDCl_3$ and analyzed either with ^1H NMR to show evidence of the peaks geminal to the functional group on the random copolymers, or with ^{31}P NMR in the case of phosphine containing RCP. In most cases, these peaks were highly diagnostic of the presence of the additional functional group. In one instance (the amine-functionalized RCP), the signal corresponding to this functional group was readily present in the RCP ^1H NMR spectrum, but not observed in the recovered sample, either due to low concentration or due to hydrogen bonding causing a shift of the weak signal to a position obscured by other peaks in the spectrum. Nevertheless, because the shift in this ^1H NMR peak relative to the starting material (the azide-functionalized RCP) was readily apparent, and because the amine-functionalized RCP caused a significant shift in the photonic band gap when incorporated into the BBCP, it is still reasonable to conclude that it is present in the BBCP array.

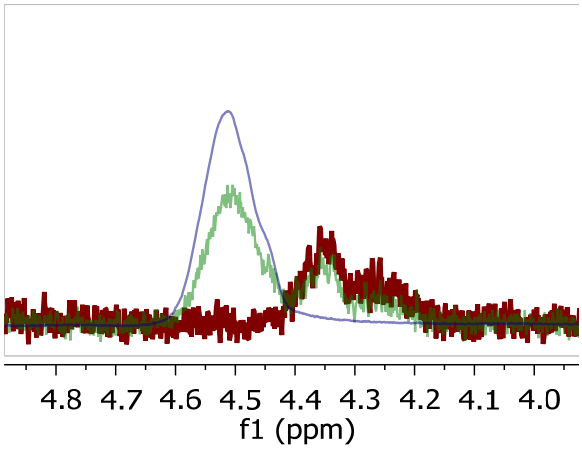

Fig. S32: ^1H NMR overlay of the P-S-VBzCl RCP (blue trace), the BBCP-PLA MM blend control (red trace), and the recovered BBCP/RCP blend (green trace), showing that both the BBCP and the RCP functional groups were present in the blend. The peak at 4.5 corresponds to the protons geminal to the chloride group.

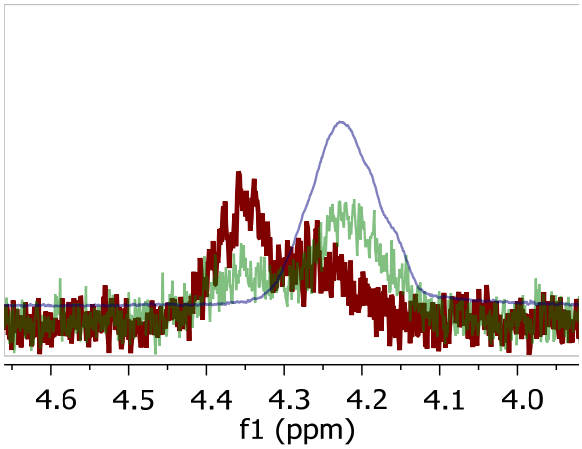

Fig. S33: ^1H NMR overlay of the P-S-N_3 RCP (blue trace), the BBCP-PLA MM blend control (red trace), and the recovered BBCP/RCP blend (green trace), showing that both the BBCP and the RCP functional groups were present in the blend. The peak at 4.2 corresponds to the protons geminal to the azide group.

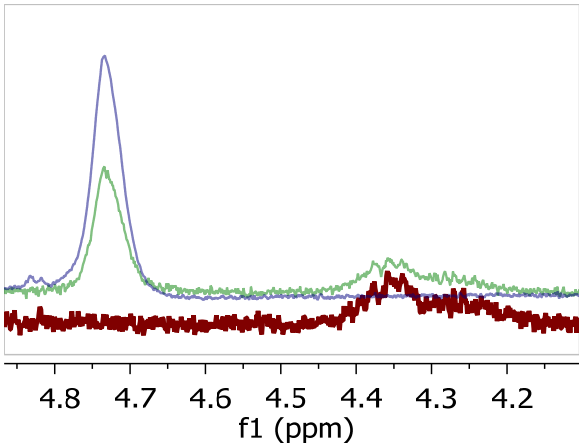

Fig. S34: ^{1}H NMR overlay of the P-S-NB RCP (blue trace), the BBCP-PLA MM blend control (red trace), and the recovered BBCP/RCP blend (green trace), showing that both the BBCP and the RCP functional groups were present in the blend. The peak at 4.75 corresponds to the protons geminal to the "clicked" triazole group.

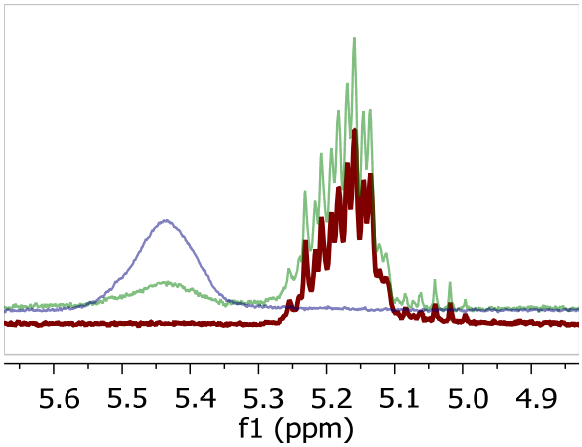

Fig. S35: ^{1}H NMR overlay of the P-S-CN RCP (blue trace), the BBCP-PLA MM blend control (red trace), and the recovered BBCP/RCP blend (green trace), showing that both the BBCP and the RCP functional groups were present in the blend. The peak at 4.75 corresponds to the protons geminal to the "clicked" triazole group.

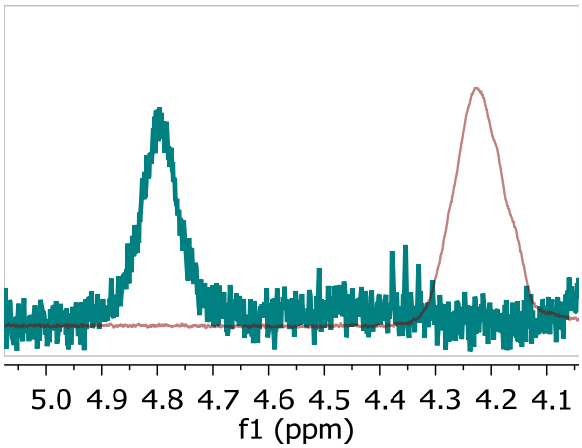

Fig. S36: ^{1}H NMR overlay of the P-S-NH_2 RCP geminal peak (blue trace) and the P-S-N_3 RCP used to synthesize the P-S-NH_2 RCP's geminal peak (red trace), indicating that the starting material was completely converted to the desired product.

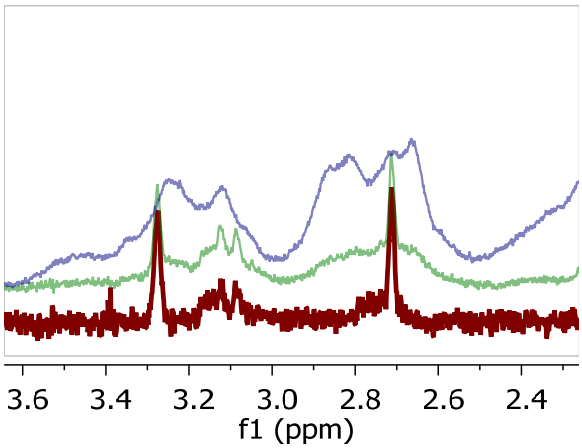

Fig. S37: Partial ^{1}H NMR overlay of the P-S-MMA RCP (blue trace), the BBCP-PLA MM blend control (red trace), and the recovered BBCP/RCP blend (green trace), showing that both the BBCP and the RCP functional groups were present in the blend.

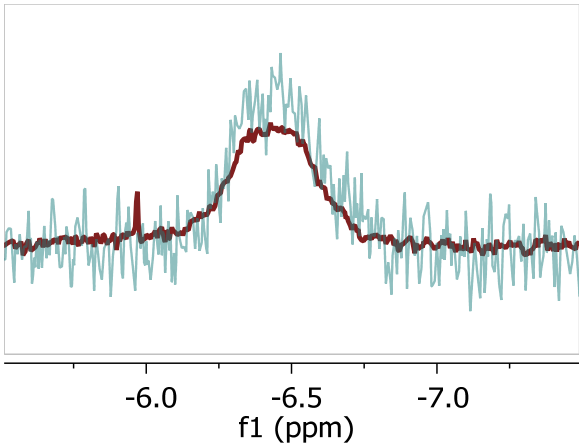

Fig. S38: ^{31}P NMR Overlay of the P-S-PPh_3 RCP (red trace) and the recovered BBCP-RCP blend, demonstrating that the RCP was indeed incorporated into the film. The peak at -6.0ppm is trace (<1%) 4-diphenylphosphinostryene that was not observed in the BBCP film.

Additional SCFT Simulation Data

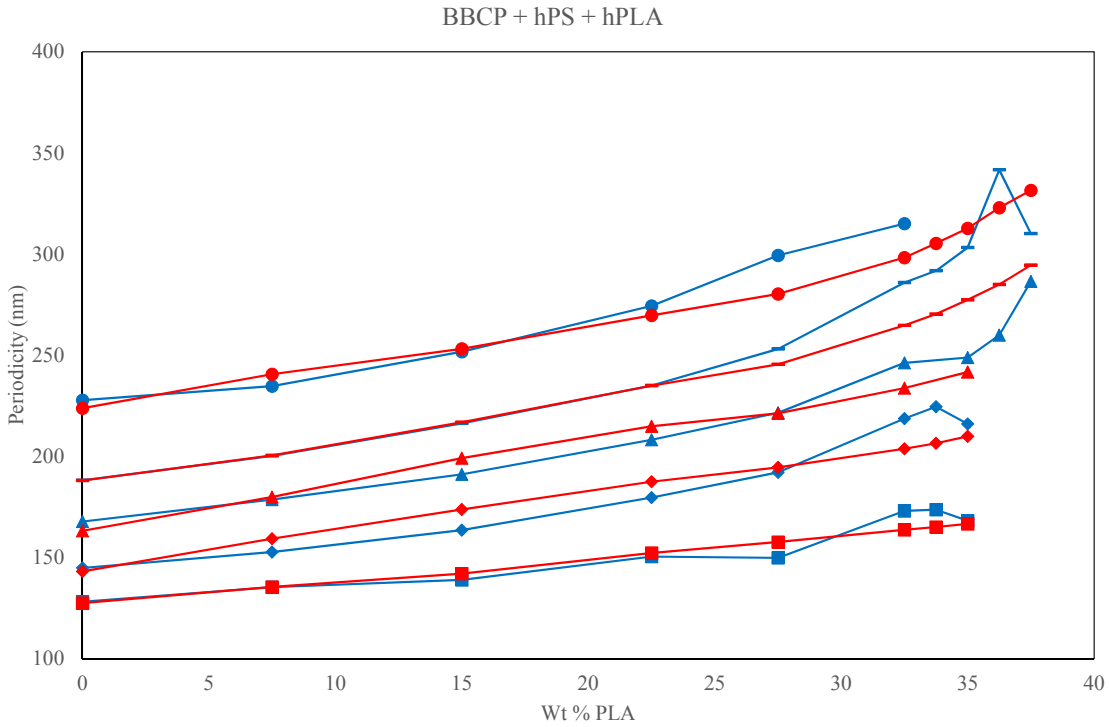

Fig. S39: Bulk periodicity as a function of the weight percent of homopolymer PLA (equal to weight % of homopolymer PS). Experimental measurements are depicted in blue and simulation results are depicted as red. From the bottom up, the square, diamond, triangle, bar and circle data points represent BBCPs with MW = 987 kDa, 1,410 kDa, 1,600 kDa, 1,760 kDa and 2,110 kDa, respectively.

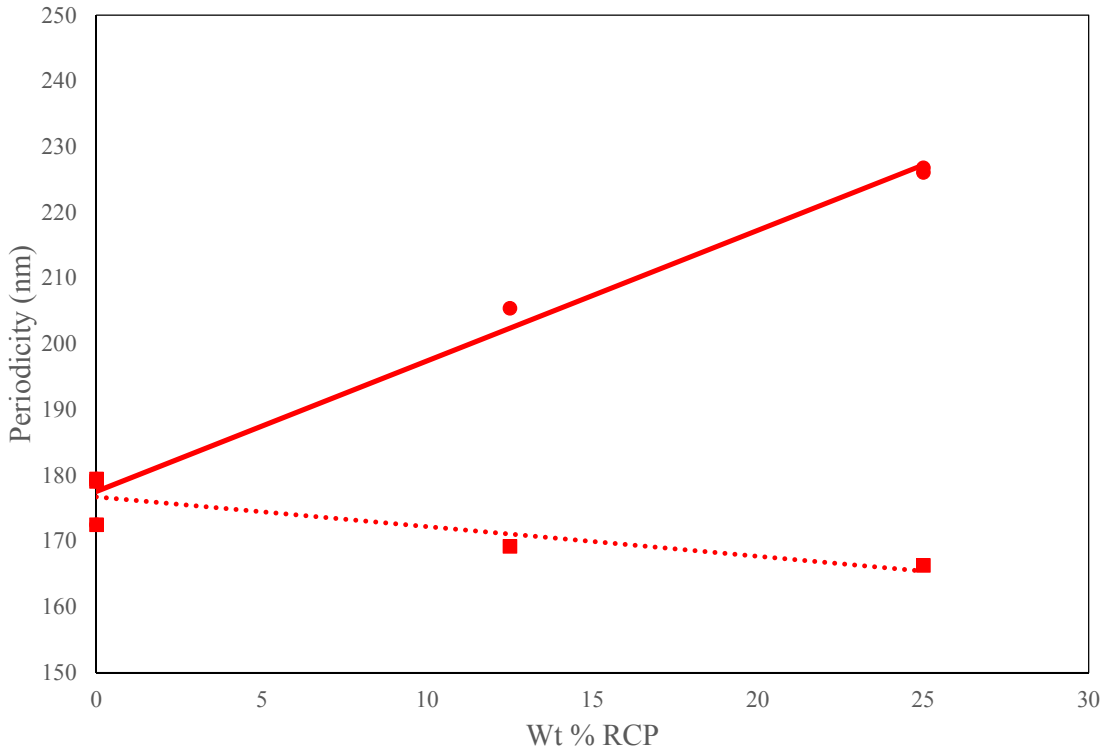

Fig. S40: Bulk periodicity as a function of the weight percent of random copolymer (RCP) (equal amounts of PLA-HP were also included in the simulation). Simulation results are depicted in two ways: circles with a solid line denoting a system where adding RCP increased lamellar periodicity, and squares with dashed line denoting a system where adding RCP decreased lamellar periodicity. The molecular weights of the polymers are 1,600 kDa for the BBCP, 3.1 kDa for PLA-HP and 6.0 kDa for RCPs. χ parameters for PS, PLA and RCPs are set as $\chi_{PS\text{-}PLA} = 12.0$, $\chi_{PS\text{-}RCP} = 3.0$, and $\chi_{PLA\text{-}RCP} = 15.0$ for the system with increasing lamellar spacing and $\chi_{PLA\text{-}RCP} = 9.0$ for the system with decreased lamellar spacing.

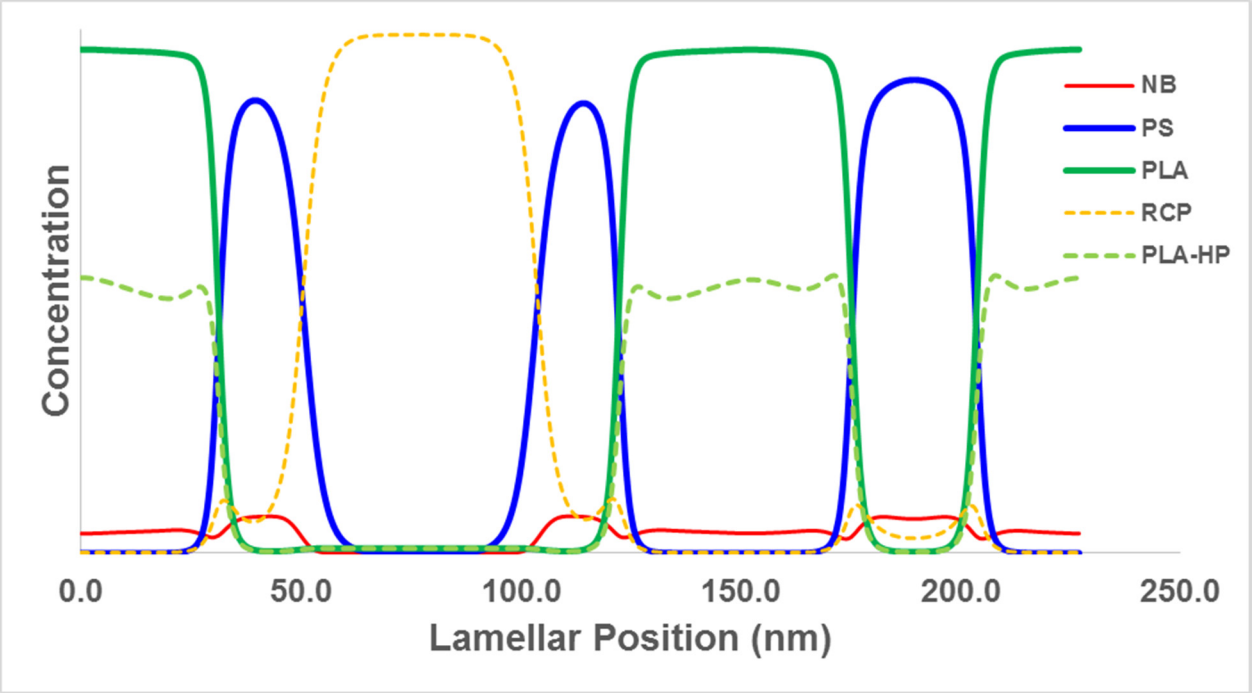

Figure S41. Locations of BBCP, RCP, and PLA-HP for a system where $\chi_{PS\text{-}PLA}$ = 12.0, $\chi_{PS\text{-}RCP}$ = 3.0, and $\chi_{PLA\text{-}RCP}$ = 15.0, and relative weight percents are 50% BBCP, 25% RCP, and 25% PLA-HP.

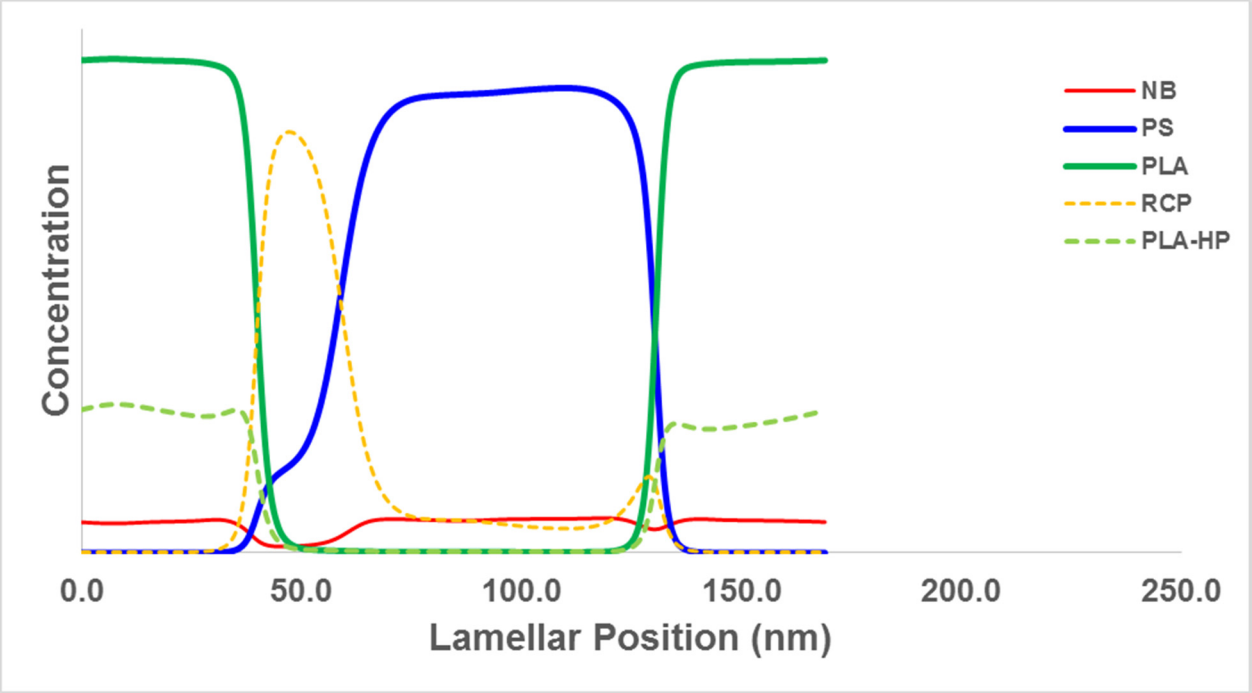

Figure S42. Locations of BBCP, RCP, and PLA-HP for a system where $\chi_{PS\text{-}PLA}$ = 12.0, $\chi_{PS\text{-}RCP}$ = 3.0, and $\chi_{PLA\text{-}RCP}$ = 9.0, and relative weight percents are 75% BBCP, 12.5% RCP, and 12.5% PLA-HP.

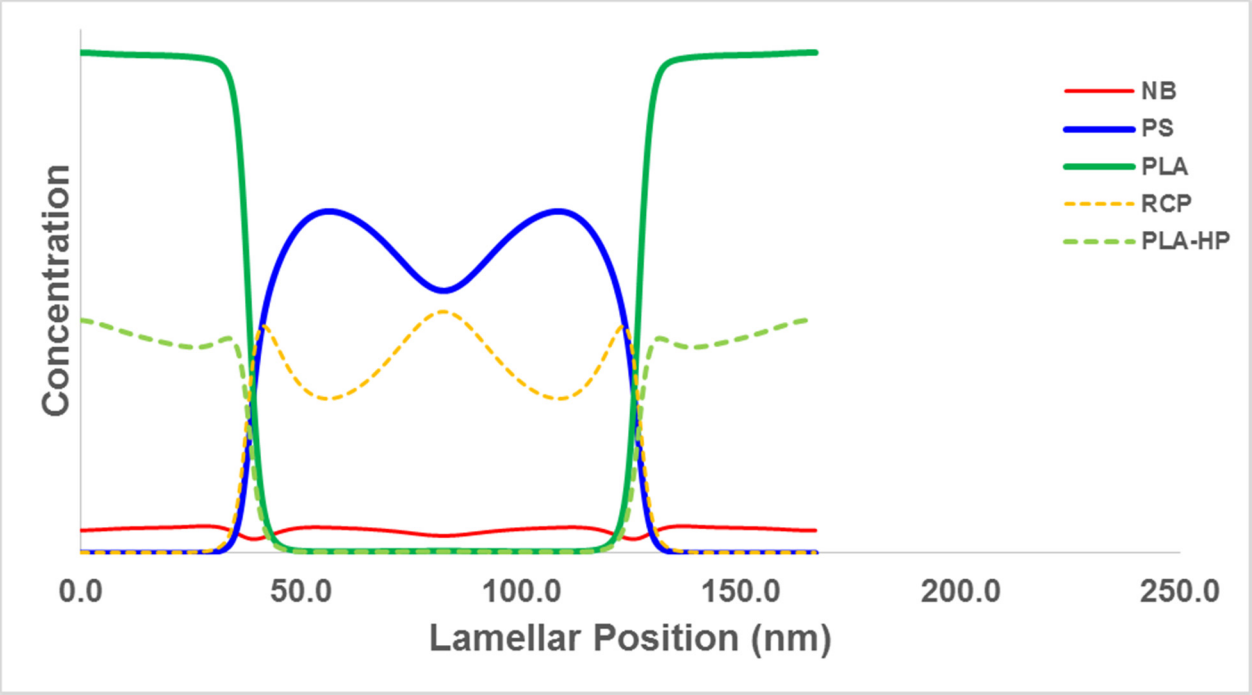

Figure S43. Locations of BBCP, RCP, and PLA-HP for a system where $\chi_{PS\text{-}PLA}$ = 12.0, $\chi_{PS\text{-}RCP}$ = 1.0, and $\chi_{PLA\text{-}RCP}$ = 9.0, and relative weight percents are 75% BBCP, 12.5% RCP, and 12.5% PLA-HP.

Modeled UV-Vis Data

The overall reflectance of a polymer film can be characterized by three metrics: the position of the band gap, the relative width of the band gap, and the absolute amount of reflectance in the film. Each of these variables is affected by the domain spacing of the lamellae, the number of repeating layers, and the degree of ordering in the film. As such, although the general quality of different films can be compared against one another using solely their reflectance properties (in the manner indicated in the main text), it is helpful to examine these properties more rigorously by modeling the optical properties of different films.

We therefore utilized Transfer Matrix Method modeling techniques to determine how the optical properties of the BBCP blend films varied with varying degrees of disorder within the film, using the resulting FWHM of the modeled films as an indication of their quality. Basic methods of these modeling techniques and code can be found in reference (1). In short, the amount of disorder was simulated by varying the domain spacing of the layers within a film by a given coefficient of variation as a means of simulating imperfect films. As the coefficient of variation increased, the photonic band gap broadened and the amount of reflectivity of the film decreased. By modifying the simulations such that the film reflectivity and photonic band gap FWHM matched the experimental data, we could determine how adding homopolymers to the films affected the overall film ordering in a semi-quantitative manner.

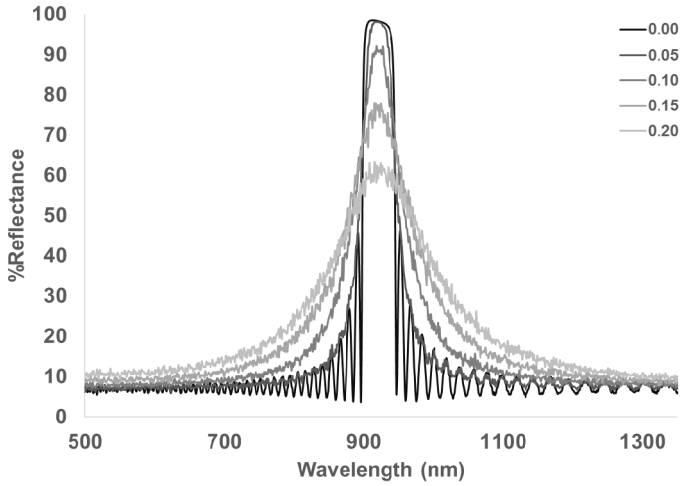

Figure S44. Modeled film reflectivities demonstrating that as the amount of disorder in the film increases (simulated as an increasing coefficient of variation in lamellar thickness), the reflectance peak broadens and the amount of reflectivity decreases.

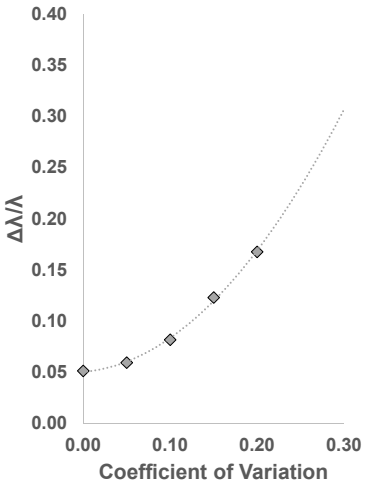

Figure S45. A plot of photonic band gap FWHM as a function of disorder in the films in fig. S44, with a trendline as a guide for the eye.

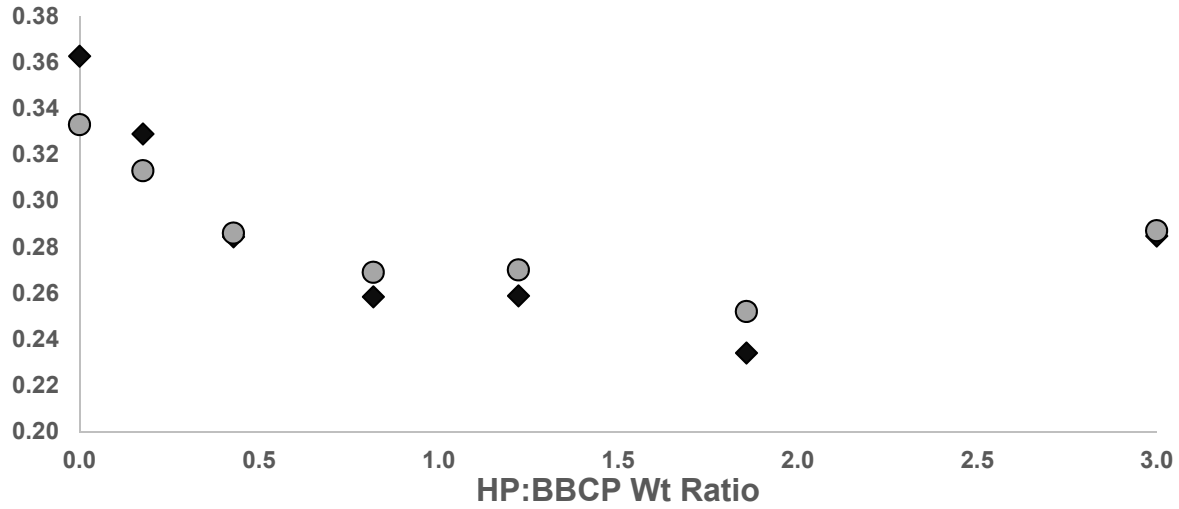

Figure S46. Comparison of experimental FWHM and the amount of variation in lamellar thickness needed to simulate the amount of disorder observed in the sample. Black diamonds are experimental FWHM values for BBCP G blends (y axis is $\Delta\lambda/\lambda$). Grey circles are the corresponding coefficient of variation in lamellar thickness needed to match the FWHM in the simulated data (y axis is the coefficient of variation). This data demonstrates that the FWHM narrowing in the experimental data is indeed an indication of improvement in BBCP film quality.

SAXS Data and Relative Lamellar Thickness

Because the photonic properties (band gap position and relative intensities and widths of band gap peaks) are dependent upon the relative thicknesses of the PS and PLA layers within an array, it is important to determine whether the layers are completely equal in width, or if there is any asymmetry in the layer thicknesses. Although the SEM data appear to show that the layers are asymmetric, these films were highly processed post assembly in order to obtain the SEM images, and it is not clear if these processing methods affected the relative thickness of the lamellae. Therefore, a more informative approach would be to examine the layer thickness *in situ* using SAXS.

To determine relative thicknesses, we scanned the samples with SAXS, then performed a Fourier synthesis transformation to determine if there was any asymmetry in the layer widths (7). From these data (fig. S47-49), we can determine that the layer thicknesses are not completely symmetric, but exhibit a thickness ratio of ~3:2. This allows us to explain why the second harmonic peak is visible in samples with large degrees of ordering (fig. 3B, fig. S3-7), despite the fact that this peak would be unobservable in a completely symmetric lamellar arrays with low refractive index contrast between layers (8).

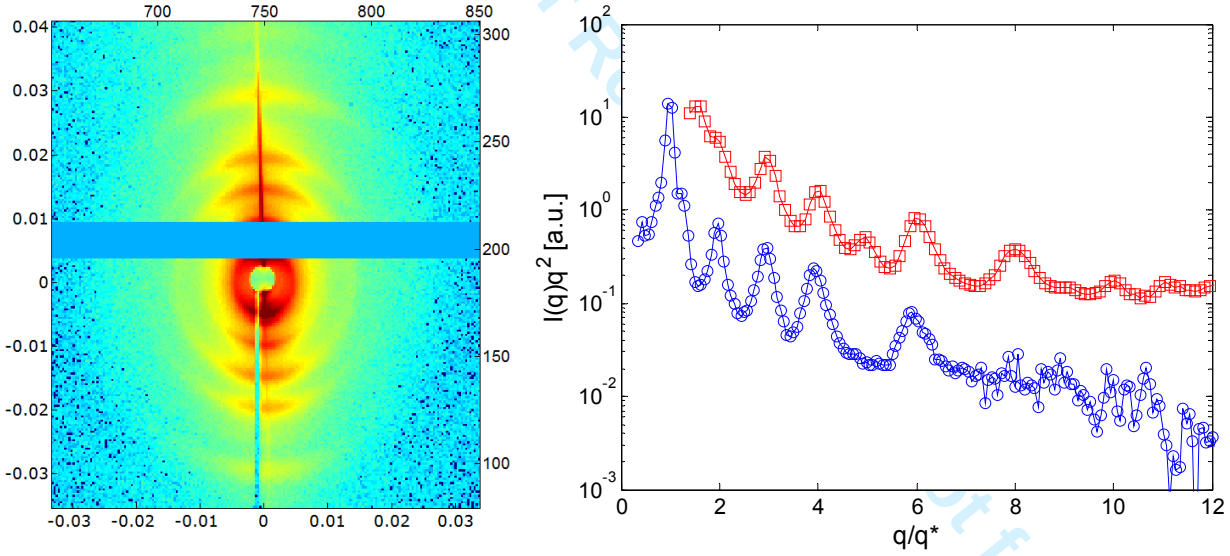

Figure S47. Left: 2D SAXS image for BBCP A, 0 wt% HP. The lamellar peaks are developed along the vertical (z) direction, indicating that lamellae are parallel to substrate. Right: Vertical line scan data for BBCP A, 0 wt% HP (blue) and BBCP A, 70 wt% HP (Red). Note that the first order peak in the 70 wt% sample is unobservable due to it being outside of the observable q range. 1D SAXS data are plotted as scattering intensity versus normalized scattering vector q (data are normalized to the position of the first order scattering peak).

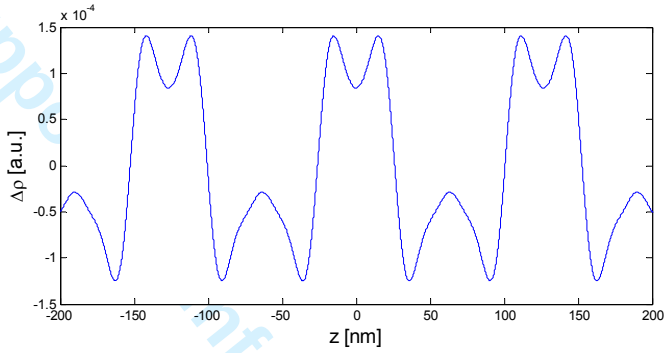

Figure S48. Fourier synthesis results for the BBCP A 0 wt% sample. The x axis is the relative lamellar position and the y axis is the relative electron density. The period obtained from this result is ~130 nm, with relative block thicknesses of ~80 nm and ~50 nm, which is approximately a 3:2 ratio. Six diffraction peaks were resolved from the SAXS data resolved and the signs of the peaks are [1, 1, -1, -1, 1, 1] for this result.

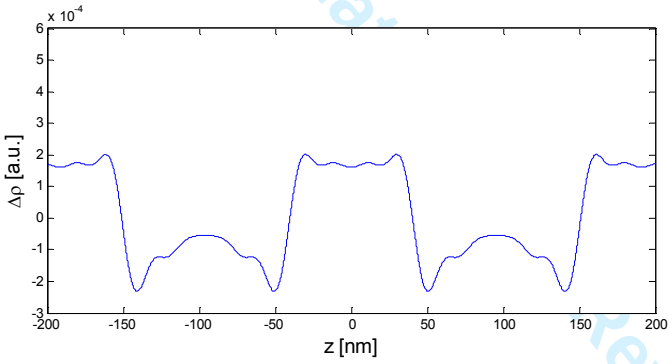

Figure S49. Fourier synthesis results for the BBCP A 70 wt% sample. The x axis is the relative lamellar position and the y axis is the relative electron density. The period obtained from this result is ~190 nm, with relative block thicknesses of ~110nm and ~80nm, or approximately a 3:2 ratio. Ten diffraction peaks were resolved from the data and the signs of the peaks are [1, 1, -1, -1, 1, 1, 1, -1, -1, 1] for this result.

To further probe the effects of asymmetry on the photonic properties of the lamellar arrays, we also simulated reflection data as a function of a varied volume fraction between the PS and PLA blocks (fig. S50). For these data, the absolute periodicity was fixed, but the relative volume fractions of PS and PLA were varied. While in the perfectly 50:50 case, the second order peak is not observable, this peak reappears even at low asymmetry (i.e. 40:60 or 60:40). The data clearly show that increasing asymmetry results in an increasing amplitude of the second order peak relative to first order peak intensity. This data is further indication that the relative layer thicknesses in the film are ~3:2 as opposed to 1:1, where the second order peak would not be observed, or highly asymmetric where the second order peak would be much more intense than is observed in the experimental data.

Additionally, a comparison of the peak position as a function of relative layer thickness for films with 50:50 PLA-PS volume fractions and 60:40 PLA-PS volume fractions shows that the experimental data is in close agreement with both simulations (table S6). However, samples with larger incorporation of homopolymers show greater discrepancy between experiment and simulation; differences in the refractive indices of the homopolymers versus the refractive indices of the brushes on the brush block copolymer could be a contributing factor to this discrepancy. Nevertheless, all simulations predict the peak of reflection within 15%, which further confirms that the simulated and experimental optical data are in good agreement with one another.

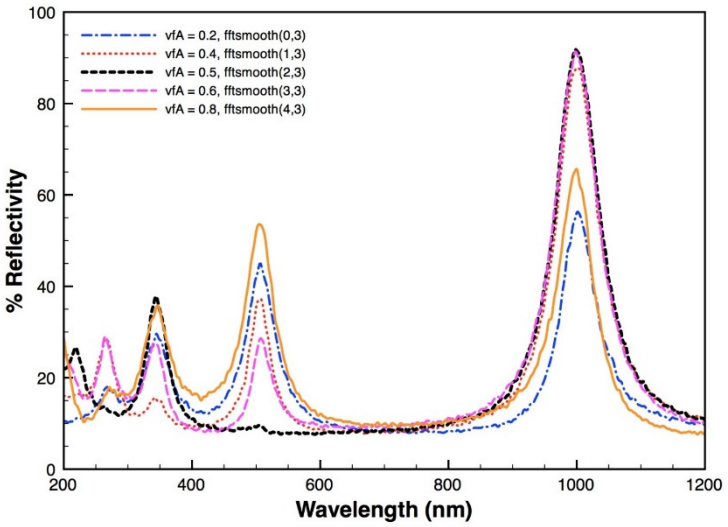

Figure S50. Modeled UV-Vis data as a function of relative layer thicknesses. In the perfectly symmetric case (black trace), the second order peak (~500 nm) is not observed, but this peak reappears when the layers are made asymmetric. The relative intensities of the peaks observed in the experimental data are more in line with layers that are slightly asymmetric (red, pink traces), rather than highly asymmetric (orange, blue traces), as in the highly asymmetric traces, the second order peak (~500 nm) is of almost equal intensity to the first order peak (~1000 nm). This is in contrast to the experimental results (fig. 3B, S3-7), where the second order peaks are always of much lower intensity than the first order peaks.

BBCP ID	Wt% HP	Lamellar Period (nm)	Measured λ_{Max} (nm)	50:50 Simulated λ_{Max} (nm)	% Difference	60:40 Simulated λ_{Max} (nm)	% Difference
BBCP A	0	128	391	393	0.51	392	0.26
BBCP A	15	134	413	412	-0.24	410	-0.73
BBCP A	30	141	424	433	2.12	430	1.42
BBCP A	45	156	459	478	4.14	474	3.27
BBCP A	55	171	457	522	14.22	518	13.35
BBCP A	65	188	528	572	8.33	569	7.77
BBCP A	67.5	197	530	599	13.02	595	12.26

Table S6. Calculated photonic band gap positions as a function of layer asymmetry. The experimentally derived lamellar spacing (as determined by SAXS) and measured photonic band gap position are compared against simulated data with perfectly symmetric layer thicknesses and layers that have a 60:40 PLA:PS volume fraction. The % difference values show the deviation between the simulated data and the experimental results.

References

(1) Sveinbjornsson, B. R.; Weitekamp, R. A.; Miyake, G. M.; Xia, Y.; Atwater, H. A.; Grubbs, R. H. **Proc. Natl. Acad. Sci. U. S. A.** 2012, *109*, 14332.

(2) Maher, M. J.; Bates, C. M.; Blachut, G.; Sirard, S.; Self, J. L.; Carlson, M. C.; Dean, L. M.; Cushen, J. D.; Durand, W. J.; Hayes, C. O.; Ellison, C. J.; Wilson, C. G. **Chem. Mater.** 2014, *26*, 1471.

(3) Xia, Y.; Kornfield, J. A.; Grubbs, R. H. **Macromolecules** 2009, *42*, 3761.

(4) Wallace, K. J.; Hanes, R.; Anslyn, E.; Morey, J.; Kilway, K. V.; Siegeld, J. **Synthesis** 2005, *12*, 2080–2083

(5) Patel, D. M.; Frederickson, G. H. **Phys. Rev. E.**, 2003, 051802

(6) Zalusky, A. S.; Olayo-Valles, R.; Wolf, J. H.; Hillmyer, M. A.; **J. Am. Chem. Soc.**, 2002, *124*, 12761.

(7) Roe, R. J., Methods of X-ray and Neutron scattering in polymer science, Oxford University Press: New York, NY, 2000.

(8) Joannopoulos, J. D.; Johnson, S. G.; Winn, J. N.; Meade, R. D. Photonic Crystals: Molding the Flow of Light; 2 ed.; Princeton University Press: Princeton, NJ, 2008.